INTERNATIONAL JOURNAL OF HYDROGEN ENERGY XXX (XXXX) XXX

Available online at www.sciencedirect.com

ScienceDirect

journal homepage: www.elsevier.com/locate/he

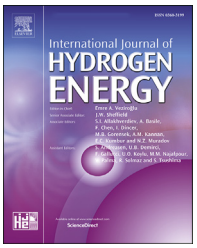

Modeling fatigue life and hydrogen embrittlement of bcc steel with unified mechanics theory

Hsiao Wei Lee [a], *Milos B. Djukic* [b], *Cemal Basaran* [a,*]

[a] *Civil, Structural, and Environmental Engineering, University at Buffalo, NY, USA*
[b] *University of Belgrade, Faculty of Mechanical Engineering, Kraljice Marije 16, Belgrade 11120, Serbia*

HIGHLIGHTS

- Unified mechanics theory is used to model the fatigue life of hydrogen embrittled low carbon steel.
- The HELP + HEDE model for hydrogen embrittlement is thoroughly reviewed, discussed and applied.
- The entropy generation equations for the multiple hydrogen embrittlement mechanisms are derived.
- Simulated stress vs. the number of cycles to failure curve (S–N) is constructed without curve fitting.
- The effects of hydrogen concentration are explained based on entropy production mechanisms.

ARTICLE INFO

Article history:
Received 19 December 2022
Received in revised form
30 January 2023
Accepted 28 February 2023
Available online xxx

Keywords:
Entropy
Unified mechanics theory
Thermodynamics
Fatigue
Hydrogen embrittlement
Steel

ABSTRACT

The fatigue life estimation of metals operating in hydrogen-rich environments such as hydrogen pipelines, hydrogen-burning internal combustion engines, etc. is important. Studies in the past 40 years have shown that the diffusion of hydrogen into steel and other metals causes various chemical reactions, hydrogen-material interactions, and microstructural changes. That leads to hydrogen embrittlement (HE) and other types of hydrogen damage mechanisms including hydrogen environmentally assisted cracking (HEAC). Hydrogen embrittlement mechanisms, such as hydrogen-enhanced localized plasticity (HELP) and hydrogen-enhanced decohesion (HEDE) can have synergetic effects in steel depending on the hydrogen concentration level. At concentrations above and below the critical hydrogen concentration, HEDE and HELP dominate the embrittlement process, respectively. Different HE mechanisms result in distinctly different fracture modes, both ductile and fully brittle. The ultrasonic vibration fatigue life of bcc steel with a ferrite-pearlite microstructure pre-charged with hydrogen at different concentrations is studied. Modeling is based on the unified mechanics theory (UMT), which does not need any empirical dissipation/degradation potential function or an empirical void evolution function. However, the UMT does require analytical derivation of the thermodynamic fundamental equation of the material, which is used to calculate the thermodynamic state index (TSI) of the material. The UMT is ab-initio unification of the second law of thermodynamics and the universal laws of motion of Newton [1]. Dissipation/degradation evolution is governed by Boltzmann's second law of thermodynamics entropy formulation. The original contribution of this paper is the derivation of the thermodynamic fundamental equation of pre-hydrogen embrittled bcc steel subjected to ultrasonic very high cycle fatigue and the numerical simulations of fatigue life estimation using the proposed novel model. The synergetic interaction of hydrogen embrittlement mechanisms in steel and other metallic materials, i.e., HELP and HEDE at different hydrogen concentrations (HELP + HEDE model)

* Corresponding author.
E-mail address: cjb@buffalo.edu (C. Basaran).
https://doi.org/10.1016/j.ijhydene.2023.02.110

is also studied, reviewed, and applied. The synergetic effects between ultrasonic vibration fatigue life and synergistically active hydrogen embrittlement mechanisms in low carbon bcc steel (S355J2+N, equivalent to ASTM A656), according to the HELP + HEDE model for HE, is modeled for the first time using UMT and also thoroughly discussed.

Introduction

Fatigue failure of components is very common in all engineering applications. Often, fatigue of the material is accelerated by other environment-assisted cracking (EAC) mechanisms [2], such as (i) corrosion (corrosion-fatigue), (ii) stress corrosion fatigue cracking, and (iii) hydrogen embrittlement - HE (including hydrogen-enhanced fatigue especially hydrogen-enhanced fatigue crack growth rate). The influence of gaseous hydrogen on fatigue life, particularly on fatigue crack growth rate (FCGR), and on fracture of hydrogen transportation steel pipelines is a very active research topic [2–6]. The reasons for intense research activity on this topic are (i) a recent trend of repurposing existing gas pipeline infrastructure that allows the injection (blending) of certain amounts of gaseous hydrogen (H_2) into a natural gas stream, and (ii) repurposing - converting existing natural gas pipelines into 100% H_2 transportation pipelines [7,8]. Unfortunately, hydrogen degrades steel with synergistically active hydrogen embrittlement mechanisms, i.e., HELP + HEDE model of HE [9–11]. A literature survey on hydrogen's detrimental effect on the fatigue life of steel is summarized in the following subsection Hydrogen embrittlement (HE) effects on fatigue for metal alloys with different microstructures. The next subsection Critical hydrogen concentration, hydrogen-dislocation interactions, and synergy of HE mechanisms, provides a review of the critical hydrogen concentration, hydrogen-dislocation interactions, and synergy of HE mechanisms. Finally, subsection The unified mechanics theory (UMT), gives a short overview of unified mechanics theory (UMT).

The studies published in the literature are mainly experimental, and the models are mainly based on Newtonian mechanics. Therefore, degradation evolution is modeled by empirical models based on curve fitting functions obtained from test data, not from the thermodynamic fundamental equation of the material. We were unable to find any physical chemistry-based fatigue life models that quantify the contribution of damage from each hydrogen embrittlement entropy generation micro-mechanism using thermodynamics. We were also unable to find any published experimental or computational study on the hydrogen embrittlement effect on ultrasonic vibration fatigue life (very high cycle fatigue life at 20 kHz). The concept of using Boltzmann's thermodynamic entropy as a degradation metric is extensively documented in Ref. [1]. Previously, it has been used extensively and successfully for thermal, electrical, chemical, or mechanical loadings but never for ultrasonic vibration fatigue of steel samples subjected to hydrogen embrittlement.

The primary aim of this study is to derive the thermodynamic fundamental equation of bcc steel with a ferrite-pearlite microstructure pre-charged with hydrogen (hydrogen embrittled) through the electrochemical method, subjected to ultrasonic vibrations. It is assumed that the fatigue test is conducted in a hydrogen-rich environment to prevent out-gassing. In UMT, degradation at a material point is quantified by the total specific entropy production rate. Because entropy is an additive property, the contributions to the total entropy production (ΔS) from all sources that operate in different stages can be added together $\Delta S = \Delta S_{corr} + \Delta S_{mec} + \Delta S_{he}$. The ΔS_{corr} is the entropy production due to corrosion during the hydrogen charging, ΔS_{mec} is the entropy production due to mechanical loading (ultrasonic vibration), and ΔS_{he} is the entropy production due to the hydrogen embrittlement mechanisms, such as HELP and HEDE, and their synergistic activities (HELP + HEDE model of HE) [9–11].

Section Thermodynamic fundamental equation presents the derivation of the thermodynamic fundamental equation. In section Entropy generation order of magnitude comparison, the order of magnitude of all the entropy generation mechanisms is discussed and compared at different ultrasonic vibration stress amplitudes. The dominant entropy generation mechanisms are determined. In section Thermodynamic state index (TSI) evolution and simulated fatigue S-N curves for the hydrogen pre-charged steel, the evolution of the TSI for hydrogen pre-charged S355J2+N steel samples subjected to ultrasonic vibration is computed at different stress amplitudes and hydrogen concentration levels. The simulated stress versus the number of cycles to failure (S–N) curves, for the hydrogen pre-charged steel (HELP + HEDE model for the synergistic action of HE mechanisms) at different hydrogen concentration levels, are plotted.

Hydrogen embrittlement (HE) effects on fatigue for metal alloys with different microstructures

Hydrogen embrittlement (HE) represents the deterioration of the mechanical properties of metals or alloys due to the presence of dissolved hydrogen in the lattice [9]. The HE usually results in the loss of ductility, the decrease of fracture toughness, the increase in fatigue fracture growth rate (FCGR), and brittle fracture failure in steel at low or subcritical stress levels [4–11]. The fatigue behavior of hydrogen embrittled steel, including the fracture toughness, fatigue crack growth rate, fatigue life, and fracture surface or crack morphology, has been studied extensively in the literature [4–8]. The external source of the hydrogen considered in these studies is mainly hydrogen that could enter the steel by either exposure

Please cite this article as: Lee HW et al., Modeling fatigue life and hydrogen embrittlement of bcc steel with unified mechanics theory, International Journal of Hydrogen Energy, https://doi.org/10.1016/j.ijhydene.2023.02.110

to a high-pressure gaseous hydrogen-rich environment or due to the cathodic charging during electrochemical corrosion.

Despite a substantial research effort dedicated to understanding the hydrogen embrittlement (HE) mechanisms in steel and various mechanisms (such as HELP and HEDE) that have been proposed, there is currently no consensus in the scientific community on the exact reason that causes the hydrogen embrittlement effect. Conflicting opinions still exist among researchers [4–11]. The specific active hydrogen embrittlement mechanism is most likely dependent on material, environmental conditions, and loading type including cyclic loading (fatigue). For hydrogen embrittlement-enhanced fatigue in steel, the HELP and HEDE mechanisms and their synergistic action according to the HELP + HEDE model proposed by Djukic et al. [9–11], and the hydrogen-induced phase transformation (HIPT) model proposed by Murakami et al. [12], especially for fcc materials, are the more widely accepted theories.

More details about the HELP + HEDE model for the synergistic action of HE mechanisms in steel depending on hydrogen concentration are given in subsection Critical hydrogen concentration, hydrogen-dislocation interactions, and synergy of HE mechanisms and subsection Synergy of different hydrogen embrittlement mechanisms. The entropy production modeled by UMT due to HE mechanisms activity, hydrogen-enhanced mechanisms HELP and HEDE, and their synergistic actions (HELP + HEDE model) in hydrogen pre-charged S355J2+N steel, is presented and analyzed in subsection Entropy production due to hydrogen-enhanced mechanisms, ΔSh, particularly in Entropy generation due to hydrogen-enhanced decohesion, ΔShede. Furthermore, a novel two-stage model for synergistic action of multiple active HE mechanisms (HELP + HEDE model) and microplasticity during very high cycle fatigue is established in subsection Entropy generation due to hydrogen-enhanced decohesion, ΔShede (see Fig. 4) and applied in this work.

Murakami et al. [12] have shown that fcc alloys such as austenitic stainless steel when subjected to hydrogen charging undergo significant microstructural changes called hydrogen-induced phase transformation (HIPT) during fracture-fatigue at the macrocrack tip in the presence of supersaturation with the hydrogen. Kishi and Takano [13] studied the effect of hydrogen cathodic charging on fatigue fracture of 310S-type austenite stainless steel. They concluded that a high concentration of dissolved hydrogen in the lattice may promote crack initiation in slip bands and decrease fatigue life. The HE mechanism during fatigue of austenitic and martensitic stainless steels was investigated by Brück et al. [14]. They proposed an empirical model that can predict the experimentally observed crack morphology and crack growth in metastable austenitic stainless steel. Their observations in samples pre-charged with hydrogen supported the theory of the HELP mechanism during short crack growth. Nahm et al. [15] investigated the very high cycle fatigue life and surface crack growth mechanism of hydrogen-embrittled AISI 304 austenitic chromium-nickel stainless steel. They concluded that the sensitivity of AISI 304 stainless steel to hydrogen gas is relatively low. They proposed an empirical surface crack initiation, growth, coalescence, and micro-ridge model. Twinning induced plasticity (TWIP) steel is austenitic steel with high content of Mn and small additions of elements such as C. Bal et al. [16] investigated the effects of hydrogen on the mechanical response and fracture locus of Fe–16Mn-0.6C-2.15Al TWIP steel at room temperature and quasi-static regime. They also observed that hydrogen enhanced the microstructural activities and changed the fracture mode from a ductile failure to brittle transgranular fracture with clear deep cracks, for TWIP steel.

For fcc alloys other than austenitic steel, Baltacioglu et al. [17] investigated the hydrogen embrittlement susceptibility of aluminum 7075 at different strain rate ranges. As opposed to their previous study in TWIP steel and austenitic stainless steel, they concluded that hydrogen embrittlement (HE) was more pronounced at high strain rate cases in aluminum 7075. They also observed that at slower strain rate hydrogen enhanced localized plasticity (HELP) was the more dominant hydrogen embrittlement mechanism. At a medium strain rate, the coexistence of HELP and HEDE mechanisms of HE was detected. A medium strain rate impact loading has also been performed on Al 7075 alloy [18]. HE was observed under impact loading. In particular, the coexistence of HE mechanisms according to the HELP + HEDE model for HE [9–11] was observed depending on the testing temperature.

Fassina et al. [19] investigated the fatigue behavior of pipeline steel at low temperatures, which has banded ferrite-pearlite microstructure and is pre-charged with hydrogen using an electrochemical method. They concluded that the hydrogen effect is influenced by load frequency and temperature. Low frequencies allow the hydrogen to migrate into the lattice at the crack tip, and consequently, the HE effects on the crack growth rate are enhanced. They also proposed that low temperature (−30 °C in their study) reduces hydrogen mobility (i.e., reduces lattice diffusion coefficient) in the lattice, hence reducing the embrittlement effect. Similar studies related to the effect of hydrogen charging on the fatigue crack growth rate during low cycle fatigue are reported by Lee and Kim [20] in SA508 Cl.3 steel with a tempered upper bainitic microstructure, and by Tsuchida et al. [21] in S45C steel with ferrite-pearlite microstructure. Rajabipour and Melchers [22] proposed an empirical model to estimate the rate of cracking of pipeline steels under hydrogen-enhanced fatigue based on the general form of Paris' law.

An et al. [23] investigated the influence of hydrogen pressure on the fatigue properties of X80 pipeline steel with ferrite and bainite microstructure, especially the fatigue crack growth rate. They concluded that hydrogen-accelerated crack initiation plays a more critical role than fatigue crack growth in reducing fatigue life with increasing hydrogen pressure. Yamabe et al. [24] investigated the effects of the hydrogen pressure, test frequency, and test temperature on the fatigue crack growth properties of annealed low-carbon steel with ferrite-pearlite microstructure. They showed that the hydrogen-enhanced fatigue crack growth acceleration always accompanied localized plastic deformations near the crack tip, and the steep gradient of the hydrogen concentration is considered to have caused localizations of the plastic deformations. Dmytrakh et al. [25] experimentally observed the effect of hydrogen concentration on fatigue crack growth in ferrite-pearlitic low-alloyed steel. It was shown that there is a characteristic value of hydrogen concentration below which

Please cite this article as: Lee HW et al., Modeling fatigue life and hydrogen embrittlement of bcc steel with unified mechanics theory, International Journal of Hydrogen Energy, https://doi.org/10.1016/j.ijhydene.2023.02.110

the FCGR reduce with increasing hydrogen concentration (an increase of crack growth resistance) and above which the FCGR increases with increasing hydrogen concentration, at a constant stress intensity factor. They proposed that such tendency results from the hydrogen-dislocation interaction: a competition between promoting dislocation pinning (or dragging) or enhancing their mobility, namely, embrittlement or enhanced plasticity. This finding correlates well with the HELP + HEDE model for HE proposed by Djukic et al. [9–11,26] which states that the transition from the HELP to HEDE mechanism dominance appears at the critical value of the hydrogen concentration. Zhao et al. [27] studied the relationship between hydrogen, peak stress of cyclic loading, and fatigue damage mechanisms on E690 high-strength, low-alloy steel with a bainitic microstructure. The electrochemical reaction is performed concurrently with cyclic loading with a 0.1 stress ratio and 0.5Hz frequency. It is shown that electrochemical hydrogen charging mainly increases the non-diffusional hydrogen concentration. This concentration is also higher at higher peak stresses due to the increasing number of hydrogen trapping sites. Because hydrogen traps are usually microscopic defects like dislocations and cavities, which can increase with higher peak cyclic stress. Different hydrogen-enhanced fatigue failure mechanisms, such as HEDE and HELP, were reported at different peak stress values and hydrogen charging current densities used during electrochemical hydrogen charging.

For steel with martensite microstructure and Ni-alloys, Balitskii et al. [28] experimentally obtained the high- and low-cycle fatigue life in high-pressure hydrogen. The hydrogen decreases the high-cycle fatigue life of martensitic steels and Ni-base alloys. Nygren et al. [29] and Oliveira et al. [30] also reported a fatigue life reduction due to hydrogen in 316L austenitic stainless steel. Vergani et al. [31] and Colombo et al. [32] investigated the hydrogen effect on the fracture toughness and fatigue behavior of AISI 4130 steel with martensite microstructure. The fatigue life curves are shifted to the left (an increase in fatigue crack growth rate - FCGR), and the fracture toughness values are reduced. The fracture surface of fatigued samples pre-charged with hydrogen is brittle and more fragmented than the specimens without hydrogen; no striations and secondary cracks are detected; in the second stage of propagation, the fracture becomes partially intergranular with secondary cracks. A comprehensive review of the impact of hydrogen embrittlement on the fatigue life of high-strength steel was published by Pradhan et al. [33]. Factors affecting hydrogen embrittlement, including the environment, applied loads, and material HE susceptibility, are thoroughly discussed. However, it should be noted that the above discussions are not general but are microstructure dependent.

The studies mentioned above explored the effect of various HE mechanisms on the fatigue life of low-carbon structural steel and other metal alloys. It is shown that the HELP mechanism leads to ductile fracture at the crack tip in almost all cases and the hydrogen-induced martensite phase transformation (HIPT) leads to brittle fracture for austenite steel. The synergistic action of (HELP + HEDE) mechanisms [9–11] and transition from the dominance of the HELP mechanism (ductile fracture) to the HEDE mechanism (brittle fracture) [26] during hydrogen-enhanced fatigue is also reported, based on critical hydrogen concentration. There are also some published experimental studies about the HE effects on ultrasonic vibration fatigue of Inconel nickel-based superalloy and 50CrV4 spring steel [34,35]. The results show increasing hydrogen concentration reduces their fatigue life significantly. Still, there are no published studies on the synergy between ultrasonic vibration fatigue and HE in low-carbon structural steel, which is the main topic of this study.

Several other researchers proposed explanations for the wildly accepted hydrogen embrittlement mechanisms (HELP and HEDE) in a thermodynamic framework. For example, Kirchheim [36–38] proposed the defactant concept to explain the influence of hydrogen on dislocations, the discontinuities (fracture surfaces, voids, dislocations) generated during hydrogen embrittlement, and the transition from ductile to brittle behavior. Kirchheim concluded that all HE models based on local plasticity caused by enhanced defects are special cases of defactant problems. Defactants segregate into defects, such as vacancies, dislocations, kinks in dislocations lines, and void or crack surfaces, and lower the critical defect formation energy in the lattice according to the generalized Gibbs relation.

Critical hydrogen concentration, hydrogen-dislocation interactions, and synergy of HE mechanisms

The stress-driven H diffusion to stress localization areas in the material and the local accumulation at key microstructural features and hydrogen trapping sites, as potential crack initiation sites are connected with the reaching so-called "critical hydrogen concentration". In HE studies of steels, the term "critical hydrogen concentration", $C_{H(\text{critical})}$, is typically connected with the sharp ductile to brittle failure transition process [9–11,26,39]. Failure mode transitions from predominantly plasticity-mediated fracture mode at lower hydrogen concentrations to the brittle fully decohesion-controlled mode typically appear upon reaching $C_{H(\text{critical})}$ [9,11,26]. However, in different published research, "critical hydrogen concentration" has been used with different physical meanings [9–11], such as:

1. A global (total) or average hydrogen concentration in the specimen.
2. Local hydrogen concentration at the trap site that causes cracking.
3. Local hydrogen concentration at a crack tip or a notch root.

Typically, in various HE studies, $C_{H(\text{critical})}$ is related to the lattice (global) hydrogen concentration or the calculated (local) hydrogen content at the particular hydrogen trap site since the measurements of the local critical hydrogen at a crack tip is challenging to conduct [40]. The critical local hydrogen concept was proved and used in numerous HE studies [9–11,26,39,41–53], while the $C_{H(\text{critical})}$ values at different length scales, local and global, depends strongly on the material, different hydrogen charging and experimental conditions, and stress/strain level. In this study, "critical hydrogen concentration" $C_{H(\text{critical})}$ defines the hydrogen content at which a ductile to brittle fracture (DBT) transition appears in the

Please cite this article as: Lee HW et al., Modeling fatigue life and hydrogen embrittlement of bcc steel with unified mechanics theory, International Journal of Hydrogen Energy, https://doi.org/10.1016/j.ijhydene.2023.02.110

presence of hydrogen in steel [9–11,26,39]. Such an interpretation is following the established and experimentally confirmed model for the simultaneous action of both the HELP and HEDE mechanisms of HE, the so-called HELP + HEDE model [9–11,26,39], depending on the hydrogen content. More details on various detected phenomena upon reaching $C_{H(critical)}$, and the transition from ductile to brittle fracture mode in steels resulting from the synergistic activity of HELP + HEDE mechanisms and the predominance of one of them depending on H concentration, was summarized in the recent comprehensive review papers [9,26].

Both HELP and HEDE mechanism can also be explained on the atomistic scale, in terms of hydrogen-dislocation interactions and hydrogen shielding effect. Murakami et al. [54] pointed out that hydrogen can have opposite effects on dislocation mobility in steel: pinning (or dragging) and enhancement of mobility depending on the hydrogen content and reaching of $C_{H(critical)}$. The enhanced dislocation mobility, i.e., HELP mechanism activity was detected over a wide range of hydrogen concentrations [40]. It provokes dislocation slip behavior around a crack tip, which leads to material softening and yield stress decreases [55–57]. Hydrogen interstitials shield (or weaken) the stress field of dislocations and effectively reduces their interactions with barriers (e.g., impurities, solute atoms, and dislocations), which is the physical basis for the plastic deformation process caused by hydrogen (HELP mechanism) [58–61]. Katzarov et al. [62] and Taketomi et al. [63] have detected both hydrogen enhancements of dislocation mobility and opposite pinning (reduction of dislocation mobility) through the atomistic modeling approach, depending on the boundary of environmental/mechanical conditions. Other important factors influencing opposite possible hydrogen-dislocation interactions are primarily local hydrogen concentration, but also applied stress/strain rate, and temperature.

On the other hand, the HEDE mechanism of HE assumes that interstitial hydrogen or hydrogen at various trapping sites (interface boundaries, grain boundaries, etc.) lowers the cohesive strength by dilatation of the atomic lattice. Its activation is based on the prerequisite that a metal's high "critical hydrogen concentration" [9–11,26,39,64] is locally reached. Wang [65] reported that the crack tip emitting dislocations, in the case of low mobility of dislocations, may behave in a brittle manner. If the motion of dislocations is impeded by hydrogen, then the shielding effects are reduced. Based on the proposed thermodynamic-kinetic model for the change in cohesion induced by hydrogen segregation, Wang [65] further indicates that activation and predominance of the HEDE mechanism may cause the ductile to brittle fracture transition in steel, which is also recently experimentally confirmed in low carbon steel [9–11,26,39]. The decohesion (HEDE) process can occur even in presence of a large amount of plastic deformation, which appeared at the crack tip fracture process zone (FPZ). In that case, the degree of the hydrogen-induced reduction in cohesion depends strongly on hydrogen mobility [65]. These observations further pointed to the importance of different hydrogen-deformation interactions, depending on the hydrogen content in metals, as well as the interconnectedness between different plasticity-mediated HE mechanisms (HELP and others) and the seemingly opposite HEDE mechanism [9].

The HELP mediated HEDE concept for the synergy of HE mechanisms introduces the significance of hydrogen-enhanced mobility/localized plasticity (HELP) as the possible previous process responsible for HEDE activation [40,58–61]. Therefore, the kinetics of transient hydrogen diffusion can be intensified due to the enhanced movements of dislocations carrying hydrogen, provoking additional hydrogen accumulation at the crack tip according to HELP and other proposed plasticity-mediated HE models. Contrary, the hydrogen-impeded mobility of dislocations, also accompanied by hydrogen-impeded localized plasticity, as a result of the opposite hydrogen-dislocation interaction upon reaching local $C_{H(critical)}$ or even higher H content at the crack FPZ, could lead to the HEDE mechanism initiation and its complete predominance ("non- HELP mediated HEDE") [9]. In such a case, according to the HELP + HEDE model for the synergistic action of the HE mechanisms in steel by Djukic et al. [9–11,26,39,64], the HEDE can be treated as a predominant HE mechanism (HELP + HEDE, HEDE >> HELP). The activity of plasticity-mediated HE mechanisms (HELP and others) on the macroscopic level can become minor, or even negligible (HEDE dominance), particularly with the increase of hydrogen content in the steel, which becomes locally much higher than $C_{H(critical)}$. The established and experimentally confirmed HELP + HEDE model for the synergy of HE mechanisms used in the study is illustrated and further elaborated in subsection Entropy generation due to hydrogen-enhanced decohesion, ΔShede.

The unified mechanics theory (UMT)

UMT has been published extensively [1,66,70–76]. In this section, we provide a summary. In Newtonian mechanics, degradation and dissipation evolution functions rely on empirical models obtained by curve fitting a function to degradation test data. Because the Newtonian space-time coordinate system does not include a linearly independent TSI axis to account for dissipation. As a result, all Newtonian mechanics-based fatigue life models are established using empirical degradation functions obtained from test data that utilize a variable such as stress, strain, or dissipated hysteresis strain energy. An extensive literature review of the most recent fatigue life prediction models was published by Lee and Basaran [66].

In the UMT [1], Newton's universal laws of motion and the second law of thermodynamics are unified at the ab-initio level. Dissipation and degradation evolve along the TSI axis between coordinates of zero and one, which is a linearly independent fifth axis, in the manner of Boltzmann (1877). It is based on Boltzmann's formulation of the second law of thermodynamics [67], in which entropy is stated to have a logarithmic connection with the disorder and was put into the final form by Planck (1901),

$$S = k_B \ln W \tag{1}$$

where S is the entropy, k_B is the Boltzmann constant, and W is the disorder parameter (probability of a microstate) [67,68]. The TSI Φ is a unitless quantity describing the difference in disorder between the original "ordered" state (or any reference state) and the current "disordered" state

Please cite this article as: Lee HW et al., Modeling fatigue life and hydrogen embrittlement of bcc steel with unified mechanics theory, International Journal of Hydrogen Energy, https://doi.org/10.1016/j.ijhydene.2023.02.110

$$s = \frac{N_A}{m_s} k_B \ln W \tag{2}$$

$$\Phi = \frac{W - W_o}{W} = \left[1 - e^{-\frac{(\Delta s) m_s}{R}}\right] \tag{3}$$

In simulations, the fatigue life is reached when

$$\Phi = \left[1 - e^{-\frac{(\Delta s_{FFE}) m_s}{R}}\right] = \Phi_{cr} \tag{4}$$

Equation (4) is an exponential function; it reaches 1 only when the power is infinite. Therefore, a critical value of the TSI near 1 is usually chosen. However, the definition of failure is application specific. Thus, the value of Φ_{cr} needs to be defined according to the problem at hand.

In equations (2)–(4), s is the entropy per unit mass (specific entropy), N_A is Avogadro's number, m_s is the molar mass, R is the universal gas constant, Δs is the change in specific entropy, Φ_{cr} is the user-defined critical value of the TSI, and Δs_{FFE} is the cumulative specific entropy at failure (also known as fatigue fracture entropy) [69]. The degradation is mapped between 0 and 1 along the TSI axis according to the cumulative specific entropy production rate of the system. The thermodynamic lifespan of any system can only be between 0 when the entropy generation rate is maximum (entropy is minimum), and near 1, when the entropy generation rate is zero (entropy is maximum), along the TSI axis. Mathematical details of the UMT are presented extensively in Ref. [1] and other publications [70–76]. Hence, the mathematical derivation of the UMT is not repeated.

Thermodynamic fundamental equation

Based on the UMT, the degradation in hydrogen pre-charged steel during ultrasonic vibration is quantified by the specific entropy production rate. Entropy is an additive property. Hence, we can add the contributions of entropy generation from all mechanisms operating in different stages together. The entropy production mechanisms can be classified into three distinct categories.

1) ΔS_{corr}, is the entropy production due to corrosion during the hydrogen charging,
2) ΔS_{mec}, is the entropy production due to mechanical loading (ultrasonic vibration),
3) ΔS_{he}, is the entropy production due to the hydrogen-enhanced mechanisms, such as the HELP and HEDE mechanisms of hydrogen embrittlement (HE), which are activated during ultrasonic vibration fatigue. The entropy production due to the work of hydrogen-induced dilatation, hydrogen transport, and the coupling of plastic strain with transient hydrogen concentrations are all included in this category.

The total entropy generation is the summation of these three main categories as follows

$$\Delta S = \Delta S_{corr} + \Delta S_{mec} + \Delta S_{he} \tag{5}$$

In the following subsections ((Entropy production due to corrosion, ΔScorr)-(Entropy production due to hydrogen-enhanced mechanisms, ΔShe)), the entropy production equations for each of the three main categories are derived. Fig. 1 shows the flowchart for numerical simulations. The definition of all variables used in the model is presented in the nomenclature.

Entropy production due to corrosion, ΔS_{corr}

There are many methods for charging steel samples with hydrogen. The most common two techniques are 1) exposure to high-pressure hydrogen gas and 2) cathodic charging from an aqueous acid solution (cathodic H charging) [77,78].

The release of hydrogen during the corrosion process is described by the following chemical reactions, [79–81].

Anodic reaction:

$$Fe \rightarrow Fe^{2+} + 2e^{-} (\text{Acid solution}) \tag{6}$$

Cathodic reaction:

$$O_2 + 4H^{+} + 4e^{-} \rightarrow 2H_2O (\text{Acid solution with sufficient oxygen})$$

$$2H^{+} + 2e^{-} \rightarrow H^2 (\text{Hydrogen evolution}) \tag{7}$$

The entropy production during electrochemical corrosion (referred to as the hydrogen-charging process in this study) has been studied extensively based on the theory of chemical kinetics and fundamentals of irreversible thermodynamics in the literature [76,81–84]. The studies show that corrosion has four primary entropy generation mechanisms. However, activation overpotential dominates the corrosion entropy production mechanisms for corrosion that happens in a well-mixed and good conductivity electrolyte [76].

Using the multiplication of thermodynamic force (electrochemical affinity) and thermodynamic flux (corrosion current densities), we can formulate the corrosion entropy production due to corrosion activation overpotential in the form of Onsager reciprocal relation [83],

$$\Delta S_{corr} = \int \frac{1}{T} \left(J_{M,a} \alpha_M z_M F\eta + J_{M,c} (1 - \alpha_M) z_M F\eta + J_{O,a} \alpha_o z_O F\eta + J_{O,c} (1 - \alpha_O) z_O F\eta\right) dt_{corr} \tag{8}$$

where T is the absolute temperature, dt_{corr} is the corrosion time (the time spend in hydrogen charging through the electrochemical method), $J_{M,a}$ and $J_{M,c}$ are the irreversible anodic and cathodic activation fluxes (thermodynamic fluxes) for the Fe oxidation reaction, respectively, $J_{O,a}$ and $J_{O,c}$ are the irreversible anodic and cathodic activation fluxes for hydrogen evolution reactions, respectively. α_M is the charge transfer coefficient for the Fe oxidation reaction, α_O is the charge transfer coefficient for hydrogen evolution reaction. z_M, and z_O are the number of valence electrons involved in reactions for the Fe and H, respectively. η is the overpotential equivalent to the difference between the applied electrode potential E and the corrosion potential E_{corr}, $\eta = E - E_{corr}$. F is Faraday's constant. $\tilde{A}_M = z_M F\eta$ and $\tilde{A}_O = z_O F\eta$ are defined as the electrochemical affinity (thermodynamic force) for Fe oxidation and hydrogen evolution induced by electrochemical overpotential, respectively. The illustration shown in Fig. 2 [85] explains the four different fluxes in equation (8).

Please cite this article as: Lee HW et al., Modeling fatigue life and hydrogen embrittlement of bcc steel with unified mechanics theory, International Journal of Hydrogen Energy, https://doi.org/10.1016/j.ijhydene.2023.02.110

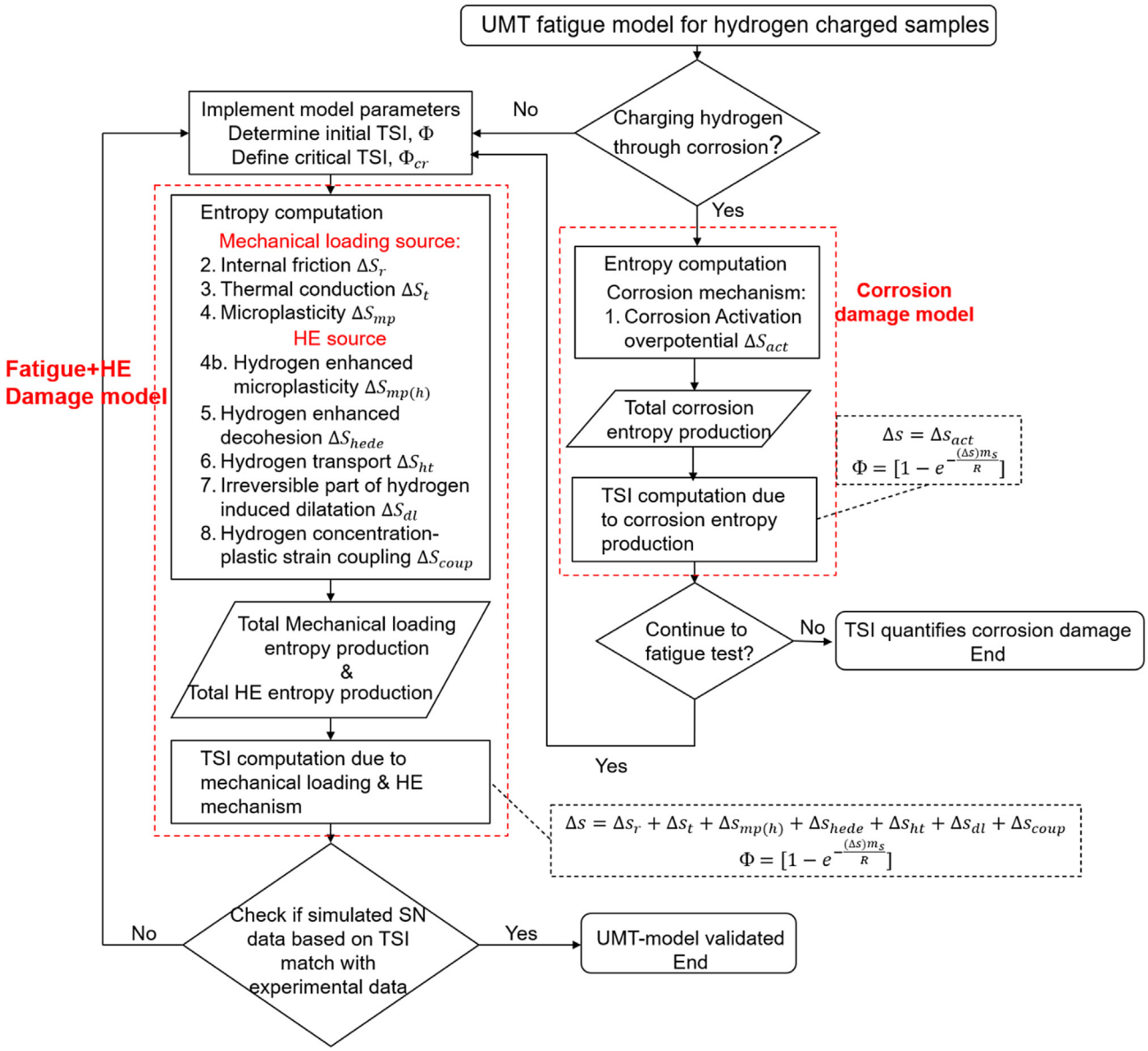

Fig. 1 – Flowchart to simulate the ultrasonic vibration fatigue life of hydrogen pre-charged steel samples.

Following the Butler-Volmer equation [80,86,87], the activation fluxes can be expressed in the following form,

$$J_M = J_{M,a} + J_{M,c} \tag{9}$$

$$J_{M,a} = j_{0,M}\left[\exp\left(\frac{\alpha_{M,a}\tilde{A}_M}{RT}\right) - 1\right];\ J_{M,c} = -j_{0,M}\left[\exp\left(\frac{-\alpha_{M,c}\tilde{A}_M}{RT}\right) - 1\right] \tag{10}$$

$$J_O = J_{O,a} + J_{O,c} \tag{11}$$

$$J_{O,a} = j_{0,R}\left[\exp\left(\frac{\alpha_{O,a}\tilde{A}_O}{RT}\right) - 1\right];\ J_{O,c} = -j_{0,R}\left[\exp\left(\frac{-\alpha_{O,c}\tilde{A}_O}{RT}\right) - 1\right] \tag{12}$$

Where J_M and J_O are the total fluxes for metal oxidation and hydrogen evolution, respectively. $j_{0,M}$ and $j_{0,R}$ are their exchange fluxes, respectively. The exchange fluxes can be expressed in the following forms: $j_{0,M} = j^0_{Fe}$, $j_{0,R} = j^0_{H_2}$ according to the chemical reactions, given by equations (6) and (7).

To utilize equation (8) and calculate the corrosion entropy production, the exchange fluxes j^0_{Fe} and $j^0_{H_2}$, the applied overpotential η, the Tafel constants α_M and α_O, and the number of valence electrons z_M and z_O are needed. The data for these variables is available in the literature on the corrosion of steel in sulfuric acid (H_2SO_4) solutions [88–92]. However, it is important to point out that NH4SCN (Ammonium Thiocyanate) is also widely used as a corrosion solution for electrochemical hydrogen charging because SCN^- accelerates hydrogen entry into steel [93–96]. In acidic conditions with the addition of acetic buffer solution, the cathodic reaction follows reaction (7) [93,94]. In contrast, in neutral conditions, and with sufficient oxygen the cathodic reaction follows $2H_2O + O_2 + 4e^- \rightarrow 4OH^-$

Please cite this article as: Lee HW et al., Modeling fatigue life and hydrogen embrittlement of bcc steel with unified mechanics theory, International Journal of Hydrogen Energy, https://doi.org/10.1016/j.ijhydene.2023.02.110

Nomenclature

Thermodynamic state index parameters			
Φ	Thermodynamic state index	Φ_{cr}	Critical thermodynamic state index
N_A	Avogadro's number	W	Disorder parameter
m_s	Molar mass	R	Universal gas constant
k_B	Boltzmann constant	Δs	Change of total specific entropy
Δs_{FFE}	Fatigue fracture entropy in the specific form		
Parameters for computation of corrosion entropy			
ΔS_{corr}	Total entropy generation due to corrosion	ΔS_{act}	Entropy generation due to corrosion activation overpotential
$J_{M,a}$	The irreversible flux of anodic half-reaction of an oxidation process	$J_{M,c}$	An irreversible flux of cathodic half-reaction of the oxidation process
$J_{O,a}$	The irreversible flux of anodic half-reaction of the reduction process	$J_{O,C}$	An irreversible flux of cathodic half-reaction of the reduction process
α_M	Charge transfer coefficient for an anodic metal oxidation reaction	α_O	Charge transfer coefficient of cathodic hydrogen evolution reaction
z_M	Effective charge number for oxidation	z_O	Effective charge number for reduction
F	Faraday's constant	η	Overpotential
E	Potential at the working electrode	E_{corr}	Corrosion potential
$\tilde{A}$	Electrochemical affinity	$\tilde{A_M}$	Electrochemical affinity for oxidation
$\tilde{A_O}$	Electrochemical affinity for reduction	j_0	Exchange flux (current density)
$j_{0,M}$	Exchange flux of oxidation process	$j_{0,R}$	Exchange flux of reduction process
j^0_{Fe}	Exchange flux of metal dissolution	$j^0_{H_2}$	Exchange flux of hydrogen evolution
I_{corr}	Corrosion current density		
Parameters for computation of mechanical loading entropy			
ΔS_{mec}	Total entropy generation due to mechanical loading	ΔS_t	Entropy generation due to thermal conduction during loading
ΔS_r	Entropy generation due to internal friction during loading	ΔS_{mp}	Entropy generation due to microplasticity during loading
k_h	Thermal conductivity	∇T	Temperature gradient
ρ	Mass density	r	The density of internal friction generated heat
ϱ	Total dislocation density	ϱ_m	Mobile dislocation density
B^{drag}	Drag coefficient	v	Dislocation velocity
G	Shear modulus (2nd Lame' constant)	b	The magnitude of the Burgers vector
α_H	Taylor's constant	$\dot{\gamma}$	Shear strain rate
Parameters for computation of HE entropy			
ΔS_{he}	Total entropy generation due to HE mechanisms	$\Delta S_{mp(h)}$	Entropy generation due to hydrogen-enhanced microplasticity
ΔS_{hede}	Entropy generation due to hydrogen-enhanced decohesion	ΔS_{ht}	Entropy generation due to hydrogen transport
ΔS_{dl}	Entropy generation due to the irreversible part of hydrogen-induced lattice dilatation	ΔS_{coup}	Entropy generation due to hydrogen coupling source
$\boldsymbol{\sigma}^{\mu}$	Microscopic stress tensor	$\boldsymbol{\varepsilon}^{\mu}_P$	The microscopic plastic strain tensor
$\boldsymbol{\sigma}^{\mu'}$	Deviatoric micro-stress tensor	$\dot{\varepsilon}_0$	Reference strain rate
$\tilde{y}$	Micro-yield stress of the material (fatigue limit)	σ^{μ}_e	von Mises effective micro-stress
$\tilde{\psi}$	The activation energy required for dislocation motion	κ^{μ}	micro flow stress over and above the micro-yield stress
f_v	The volume fraction of activated micro- defects	$\tilde{H}$	Hardening coefficient
$2\gamma_{int}$	Ideal work to fracture for the HEDE process	Ψ_f	Frequency coefficient
Δg_i	Gibbs's free energy parameter	$(2\gamma_{int})_0$	Ideal work to fracture without H
$2\gamma_s$	Free surface energy in the absence of H	Δg_s	Gibbs's free energy parameter
Γ	Interface coverage by H for decohesion	γ_i	Carbide/matrix interface energy in the absence of H_2
$A\ q$	Parameters relating $2\gamma_{int}$ to γ_p	Γ_{max}	Maximum interface coverage by H
$h_{a/v}$	Surface area to volume ratio	γ_p	Plastic work attendant in decohesion
V_H	Partial molar volume of hydrogen	$\dot{\boldsymbol{\varepsilon}}^{\mathbf{h}}$	Hydrogen concentration induced lattice dilation strain rate
J_h	Hydrogen flux	λ	Dilatation induced by a hydrogen solute in the host lattice
D	Hydrogen lattice diffusion coefficient	μ_h	The chemical potential of the hydrogen solute atoms

Please cite this article as: Lee HW et al., Modeling fatigue life and hydrogen embrittlement of bcc steel with unified mechanics theory, International Journal of Hydrogen Energy, https://doi.org/10.1016/j.ijhydene.2023.02.110

C_T	Hydrogen concentration in trapping sites	C_L	Hydrogen concentration in normal interstitial lattice sites (NILS)
θ_T	Hydrogen occupancy in trapping sites	θ_L	Hydrogen occupancy in NILS
N_T	Density of the trapping sites	N_L	Density of the host metal lattice
α	Number of trapping sites per trap	β	Number of lattice sites per solvent atom
C_L^0	Hydrogen concentration in NILS at a stress-free state	W_B	Trapping binding energy
C_0	The range of C_T	V_M	Molar volume of the host lattice
σ_H	Hydrostatic stress	$\overline{V}_H$	Partial molar volume of hydrogen in solids solution
Y_0	Initial yield stress	K_κ	Dimensionless material constant
		γ_b	The external scalar body force

[95,96]. In this study, we focused the corrosion entropy production in H_2SO_4 solution because we do not find suitable electrochemical data for low carbon steel in NH4SCN solution.

Entropy production due to mechanical loading (ultrasonic vibration), ΔS_{mec}

The entropy generation during ultrasonic vibration has been studied extensively [75]. It was shown that the mechanisms of thermal conduction, internal friction, and microplasticity are the main contributors to total entropy production,

$$\Delta S_{mec} = \Delta S_t + \Delta S_r + \Delta S_{mp} \tag{13}$$

where ΔS_t is the entropy generation due to thermal conduction, ΔS_r is entropy production due to internal friction, and ΔS_{mp} is entropy production due to microplasticity. This section focuses only on the entropy generation due to thermal conduction ΔS_T and internal friction ΔS_r. The microplastic strain and the entropy generation due to microplasticity ΔS_{mp} are enhanced when hydrogen in trapping sites is considered, according to the HELP mechanism of hydrogen embrittlement [9–11]. Therefore, the microplasticity entropy generation ΔS_{mp} will be discussed in a later subsection Entropy production due to hydrogen-enhanced mechanisms, ΔShe, where entropy production due to the hydrogen embrittlement mechanisms ΔS_{he} (hydrogen-enhanced mechanisms) are discussed.

Entropy generation due to thermal conduction, ΔS_t

During ultrasonic vibration fatigue, the surface temperature at the sample's gage section increases from 300K to 400K before the initiation of macro cracks [75]. The surface temperature gradient on the sample results in an irreversible heat flow that contributes to entropy production. The entropy production equation of this source is expressed by:

$$\Delta S_t = \int_{t_0}^{t} \frac{k_h}{T^2} (\nabla T \cdot \nabla T) dt \tag{14}$$

where k_h is the coefficient of heat conduction, and ∇T is the gradient of the sample's surface temperature from the gage section to the grip section. Equation (14) is essentially the product of temperature gradient (thermodynamic force) ∇T and heat flux (thermodynamic flux) $\boldsymbol{q} = -k_h \nabla T$.

Entropy generation due to internal friction, ΔS_r

The strain rate during ultrasonic vibration fatigue (20 kHz) is three orders of magnitude larger than typical high-cycle fatigue testing using the servo-hydraulic machine. The strain rate strongly affects entropy production due to internal friction [75], which is driven by.

1) The fast-moving dislocations during the high strain rate loading. It is derived from the rate-dependent dislocation plasticity, which postulates that driving stress for dislocation motion is the effective shear stress, against the resistance of dislocation slip shear stress [97–100].
2) The drag (friction due to scattering) process involves phonon, electron, and radiation drag [101]. At high strain rates, in addition to dislocation-dislocation interactions, the mechanism of viscous drag due to interactions with

Please cite this article as: Lee HW et al., Modeling fatigue life and hydrogen embrittlement of bcc steel with unified mechanics theory, International Journal of Hydrogen Energy, https://doi.org/10.1016/j.ijhydene.2023.02.110

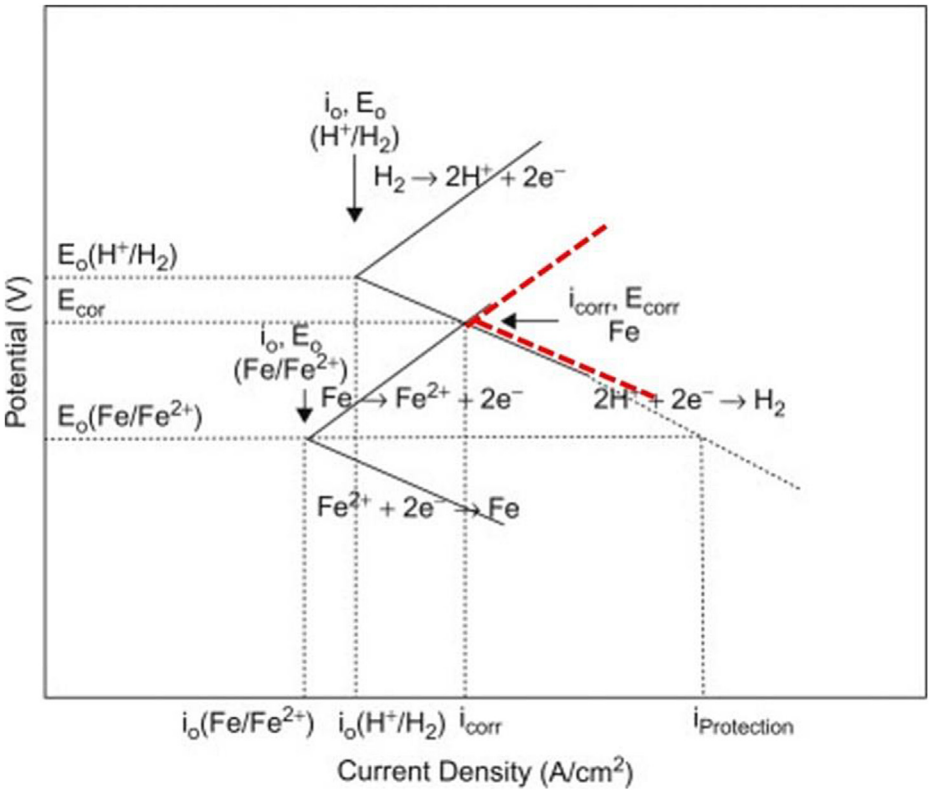

Fig. 2 – Evans diagram based on the mixed potential theory showing the iron corrosion reaction in an acid solution, adapted from Ref. [85]. The red dashed line in the middle constructs the Tafel plot, which is crucial for the determination of electrochemical properties. (For interpretation of the references to color in this figure legend, the reader is referred to the Web version of this article.)

phonons comes into play. In the field of quantum mechanics, phonons are quantitative descriptions of lattice vibrations. Gliding dislocations scatter the thermal phonons in a crystal, resulting in a drag force on the dislocations [101].

Therefore, the entropy production equation for internal friction is expressed by:

$$\Delta S_r = \int_{t_0}^{t} \frac{\rho r}{T} dt = \int_{t_0}^{t} \frac{\left(\varrho B^{drag} v^2 + \frac{1}{2} G b^2 \dot{\varrho} - \alpha_H G b \sqrt{\varrho}\, \dot{\gamma}\right)}{T} dt \quad (15)$$

where ρ is the mass density, r is the density of internal heat generation, B^{drag} and v represent the effective drag coefficient and velocity of dislocation, respectively. The variables G, b, ϱ, and α_H are the shear modulus, the magnitude of Burger's vector, total dislocation density, and Taylor's hardening parameter, respectively. In equation (15), the velocity of dislocation is related to the applied shear strain rate, $\dot{\gamma}$ as follows, equation (16):

$$v = \frac{\dot{\gamma}}{\varrho_m b} \quad (16)$$

where ϱ_m is the density of mobile dislocations. It can be observed that the dislocation drag force per unit length is $F = B^{drag} v$. Therefore, the term $\varrho F v = \varrho B^{drag} v^2$ represents the energy dissipation per unit of time.

Entropy production due to hydrogen-enhanced mechanisms, ΔS_{he}

Synergy of different hydrogen embrittlement mechanisms

When metal is exposed to a hydrogen-rich environment during forming, coating, plating, and cleaning in the manufacturing stage (source of internal hydrogen) or subjected to long-term gaseous hydrogen pressure during the exploitation (source of external hydrogen), such as hydrogen gas pipelines, the material degradation resulting from the trapping or diffusion of hydrogen into the metal is widely known as hydrogen embrittlement [9–11,26,77,78,102–106]. There have been extensive studies in the past 40 years on proposing mechanisms to explain hydrogen embrittlement, including the hydrogen pressure theory [107,108], hydrogen-induced phase transformation (HIPT) [109,110], HEDE [8–10,26,78,111–114], HELP [9–11,26,106,115–119], and hydrogen-enhanced strain-induced vacancies (HESIV) [120–122]. Despite various proposed HE mechanisms, there is currently no consensus in the literature on the inherent nature of the HE mechanism and a general HE model [9–11,26]. In this study, the emphasis is given to the HELP and HEDE mechanisms of hydrogen embrittlement and their synergistic action in a cooperating manner (HELP + HEDE model) [9–11,26,39,104,128]. Because these mechanisms are widely accepted as viable hydrogen embrittlement mechanisms that affect the fatigue life of ferrite-pearlite steel [123–125].

Please cite this article as: Lee HW et al., Modeling fatigue life and hydrogen embrittlement of bcc steel with unified mechanics theory, International Journal of Hydrogen Energy, https://doi.org/10.1016/j.ijhydene.2023.02.110

The HELP mechanism is proposed based on the in-situ observation by transmission electron microscopy (TEM) about the enhanced dislocation movement by hydrogen (HELP) [9,106,126–128]. According to the HELP mechanism, dislocation mobility (generation and motion) and dislocation slip behavior are facilitated by the hydrogen solute atoms, leading to the increase in dislocation velocity for a given applied shear stress or lower the critical shear stress required to initiate the slip of dislocations [106,118,126–128]. Eventually, it causes local dislocation pileups at defects with premature failure of the material [106,118]. The plasticity of the metal plays a significant role in the hydrogen-assisted fracture according to the HELP mechanism.

On the other hand, the HEDE mechanism is mainly based on the observed brittle intergranular fracture surfaces of metallic materials and also theoretical calculations [9–11,26]. The high accumulation of hydrogen atoms at regions such as interstitials, various hydrogen traps, dislocation shielding region at the crack tip, maximum hydrostatic stress sites, grain boundaries, phase boundaries, precipitates, etc, locally reduce the cohesive strength of metal and thus the necessary energy to fracture [9–11,26,78,105,111–114,128,129]. The HEDE mechanism has been used to develop predictive cohesive models that simulate material's cohesive strength in front of a propagating crack [9–11,103,106,112,113].

The synergistic action of HELP and HEDE mechanisms of hydrogen embrittlement in metallic materials have been studied extensively in the literature [9–11,26,39,102–104,128]. In a recent critical review paper by Djukic et al. [9] about the synergistic action and interplay of HE mechanisms in steel and iron, various HE models are classified into four categories: 1) hydrogen-enhanced plasticity models (i.e., HELP, HESIV, and others), 2) hydrogen-enhanced decohesion model (HEDE), 3) HELP mediated HEDE model [40], which assumed that these mechanisms work in collaboration, HELP provokes HEDE mechanism, and 4) A HELP + HEDE model [11,26,39,64,104,128] assuming that HELP and HEDE mechanisms are working synergistically but one of them predominates depending on the global/local hydrogen concentration and other factors.

This study uses the third and fourth hydrogen embrittlement models to simulate the interaction of HELP and HEDE mechanisms. It was recently shown through experimental studies that the HELP mechanism is not always a prerequisite for eventual HEDE activation for many metals [9], particularly at high global/local hydrogen concentrations in metallic materials. Instead, they can coexist and have synergistic interactions depending on the hydrogen concentration, for materials such as ferrite-based low carbon steel with bcc microstructure and other steel grades [9–11,26,39,78,104,128]. SEM micrographs of fractured surfaces show that there is a transition of the fracture mode from the ductile micro void coalescence (MVC) mode [with reduced dimple size due to the dominance of HELP] to brittle "quasi-cleavage" (CQ), transgranular (TG), and intergranular (IG) fracture mode due to dominance of HEDE mechanism [9,11,26,78,104,128]. This transition is assumed to occur upon the hydrogen concentration level reaching a critical value (called critical hydrogen concentration, $C_{H(\text{critical})}$) [9,10,26,39,104,130,131]. Below the $C_{H(\text{critical})}$, the HELP mechanism is dominant. Above the $C_{H(\text{critical})}$, the HEDE mechanism becomes dominant [9–11,26,78,104,128].

The entropy production due to hydrogen-enhanced mechanisms, the synergistic action, and the interplay of HE mechanisms (HELP + HEDE) during fatigue is discussed in the next subsection Entropy production due to the synergistic action of HE mechanisms.

Entropy production due to the synergistic action of HE mechanisms

Novak et al. [132,133] proposed a dislocation-based rate-dependent plasticity model within the framework of the synergistic action of HELP and HEDE mechanisms (HELP mediated HEDE model [106,118]), which incorporated the effect of hydrogen on dislocation generation, motion, and annihilation for structural steel. Utilizing the mass balance of hydrogen, the force equilibrium equation, the first and second laws of thermodynamics, the Clausius-Duhem inequality, and the Coleman-Noll procedure, they derived the constitutive equations and the dissipation in the equality equation. The dissipation inequality equation is given as follows [132,133]:

$$\boldsymbol{\sigma} : \dot{\boldsymbol{\varepsilon}}^p + \left[\boldsymbol{\sigma} : \dot{\boldsymbol{\varepsilon}}^h\right]_{\text{irr}} - \kappa\dot{\varepsilon}_{\text{ss}} - \frac{1}{T}\boldsymbol{q}\cdot\nabla \text{T} - \boldsymbol{J}\cdot\nabla\mu + (\gamma_b + \mu_h)\alpha\theta_T\frac{\partial N_T}{\partial \varepsilon^p}\dot{\varepsilon}^p \geq 0 \tag{17}$$

In which $\boldsymbol{\sigma}$ is the stress tensor, $\boldsymbol{\varepsilon}^p$ the plastic strain tensor, $\boldsymbol{\varepsilon}^h$ is the hydrogen-induced strain tensor, κ is the flow stress of the material, $\boldsymbol{\varepsilon}_{ss}$ is the lattice strain due to statistically stored dislocations (SSD), T is the absolute temperature, $\boldsymbol{q}$ is the heat flux, $\boldsymbol{J}$ is the flux of hydrogen transport (i.e., atoms passing through per unit area per unit time through the surface), and μ_h is the chemical potential of the hydrogen solute atoms. Further, γ_b is an external scalar body force, α is the number of available lattice trapping sites per trap, θ_T is the occupancy rate of hydrogen atoms in the trapping sites, and N_T is the density of traps measured in traps per unit volume.

Equation (17) provides the basis for the entropy calculation due to the HELP mechanism. The focus of this study is the very high cycle fatigue behavior of hydrogen pre-charged steel. The stress amplitude is well below the material's nominal yield stress. Therefore, the irreversible dissipation from lattice strain $\kappa\dot{\varepsilon}_{\text{ss}}$ due to SSD can be ignored. The dissipation from macro-plastic work $\boldsymbol{\sigma} : \dot{\boldsymbol{\varepsilon}}^p$ should be modified to account for micro-plastic work that happens at defect sites locally.

The entropy generation due to the HEDE mechanism must be included when considering the synergistic activity of the HELP and HEDE mechanisms [9]. As a result, in the case of ultrasonic vibration fatigue, the entropy production due to hydrogen-enhanced mechanisms ΔS_{he} can be written as the summation of five entropy generation sources,

$$\Delta S_{he} = \Delta S_{mp} + \Delta S_{hede} + \Delta S_{dl} + \Delta S_{ht} + \Delta S_{coup} \tag{18}$$

where ΔS_{mp} is the entropy generation due to hydrogen-enhanced micro-plasticity (HEL(M)P), ΔS_{hede} is the entropy generation due to the HE process of HEDE, ΔS_{dl} is the entropy generation due to the work of hydrogen-induced dilatation, ΔS_{ht} is the entropy generation due to hydrogen transport, and ΔS_{coup} is the entropy generation due to the coupling of plastic strain with transient hydrogen concentrations.

Please cite this article as: Lee HW et al., Modeling fatigue life and hydrogen embrittlement of bcc steel with unified mechanics theory, International Journal of Hydrogen Energy, https://doi.org/10.1016/j.ijhydene.2023.02.110

Entropy generation due to hydrogen-enhanced micro-plasticity, ΔS_{mp}. The microplasticity model used here is a two-scale model that considers a global elastic matrix and localized plastic inclusions at lattice defect sites due to stress concentration [75]. The microplastic mechanism is activated when the applied stress amplitude is above the fatigue limit (microscopic yield stress) but below the nominal yield stress. The entropy generation equation of this mechanism is given by Ref. [75]:

$$\Delta S_{mp} = \int_{t_0}^{t} \Psi_f \left(\Phi f_v \frac{\boldsymbol{\sigma}^{\mu} : \dot{\boldsymbol{\varepsilon}}_P^{\mu}}{T} \right) dt \tag{19}$$

where Ψ_f is a loading frequency coefficient, Φ is the TSI to account for the evolution of activated microdefects during the loading and f_v is the volume fraction of activated microdefects experiencing microplasticity, which is represented by the relative surface ratio covered by activated micro slip bands at the center of the samples' gauge part. $\boldsymbol{\sigma}^{\mu}$ and $\boldsymbol{\varepsilon}_P^{\mu}$ are the micro-stress and microplastic strain at lattice defect sites, and T is the absolute temperature on the gage surface of the sample. Generally speaking, this hydrogen-enhanced microplasticity belongs in the category of HELP. However, since this study focused especially on the elastic fatigue regime which does not generate global plastic strain, we use HEL(M)P to account for the term hydrogen-enhanced "microplasticity".

Fig. 3 shows the illustration of microplasticity. Inside the hexagon region, micro-stress and microplastic strain at each inclusion are computed under the same laws of localization and homogenization. Typically, the activated lattice defect sites during ultrasonic vibration are inclusions, vacancies, and dislocations. In the presence of hydrogen, the term "defect" also includes the interstitial and trapped hydrogen atoms. Our previous studies show that the volume fraction of activated microdefects experiencing microplasticity f_v is around 20% for uncorroded samples. It can rise above 25% for corroded samples [76].

The micro-stresses $\boldsymbol{\sigma}^{\mu}$ can be calculated by using the law of localization and homogenization based on the two-scale model [75],

$$\boldsymbol{\sigma}^{\mu} = \boldsymbol{\sigma} - \left[\frac{E(5\nu - 7)}{15(\nu^2 - 1)} \right] (1 - f_v) \boldsymbol{\varepsilon}_P^{\mu} \tag{20}$$

where $\boldsymbol{\sigma}$ is the macroscopic stress tensor, ν is Poisson's ratio, E is Young's modulus.

For the HELP mechanism, the increasing concentration of hydrogen at trapping sites specifically in the Cottrell field of the dislocation decreases the activation energy for dislocation motion, increasing the deformation in localized regions near the fracture surface [106,118]. The hydrogen-enhanced plastic strain rate $\dot{\boldsymbol{\varepsilon}}^{\boldsymbol{p}}$ is expressed by the following relation [132,133]:

$$\dot{\boldsymbol{\varepsilon}}^{\boldsymbol{p}} = \dot{\varepsilon}_0 \sinh \left[\tilde{\Psi} \left(\frac{\sigma_e}{\tilde{Y} + \kappa} - 1 \right)^n \right] \frac{\boldsymbol{\sigma}'}{\sigma_e} \tag{21}$$

where $\dot{\varepsilon}_0$ is a reference strain rate, $\boldsymbol{\sigma}'$ is the deviatoric stress, σ_e is the von Mises stress, and $\tilde{\Psi}$ is a positive dimensionless activation energy parameter as a decreasing function of hydrogen concentration, which is used to account for the effect of the activation energy required for dislocation motion. $\tilde{Y}$ is the initial yield stress of the material, as a function of hydrogen concentration. κ is the flow stress over and above the initial yield stress, and n is the hardening exponent. Assuming the microplastic strain is enhanced by the hydrogen concentration through the same function, as shown in equation (21), we can write the hydrogen-enhanced microplastic strain rate, as follows:

$$\dot{\boldsymbol{\varepsilon}}_P^{\mu} = \dot{\varepsilon}_0 \sinh \left[\tilde{\Psi} \left(\frac{\sigma_e^{\mu}}{\tilde{y} + \kappa^{\mu}} - 1 \right)^n \right] \frac{\boldsymbol{\sigma}^{\mu'}}{\sigma_e^{\mu}} \tag{22}$$

Where $\boldsymbol{\sigma}^{\mu'}$ is the deviatoric micro-stress tensor, σ_e^{μ} is the von Mises effective micro-stress, and $\tilde{y}$ is the initial micro-yield stress of the material, as a function of hydrogen concentration. κ^{μ} is the micro flow stress over and above the initial micro-yield stress. The evolution of the flow stress is given by

$$\dot{\kappa}^{\mu} = [\tilde{H} - \tilde{R} \cdot \kappa^{\mu}] \dot{\varepsilon}_p^{\mu} \tag{23}$$

where $\tilde{H}$ is the hardening coefficient and $\tilde{R}$ is the dynamic recovery coefficient, both are functions of hydrogen concentration.

The material parameters as a function of hydrogen concentration in trapping sites, C_T in equations (22) and (23) are expressed by the following relations [132,133],

$$\tilde{\Psi}(C) = \Psi_0 \left(1 + \Psi_c \frac{C_T}{C_0} \right) \tag{24}$$

$$\tilde{y}(C) = y_0 \left(1 + y_c \frac{C_T}{C_0} \right) \tag{25}$$

$$\tilde{H}(C) = H_0 \left(1 + H_c \frac{C_T}{C_0} \right) \tag{26}$$

where C_T/C_0 is the normalized hydrogen concentration in trapping lattice sites, C_0 is the possible range of C_T. Ψ_c, y_c, and H_c are positive dimensionless constants representing the hydrogen-induced plastic softening, the blocking of Frank-Read dislocation sources by hydrogen, and the hydrogen-assisted hardening, respectively [132]. They can be experimentally measured by pre-charging a test sample to $C_T = C_o$ level, then obtaining $H_c = (\tilde{H} - H_0)/H_0$ when $C_T = C_0$. The required material constants mentioned above for the calculation of HEL(M)P entropy production in S355J2+N steel are presented in Table 2, Hydrogen enhanced microplastic strain rate function parameters.

Entropy generation due to hydrogen-enhanced decohesion, ΔS_{hede}. A physics-based statistical micro-mechanical model of the hydrogen-induced intergranular fracture in steel was introduced by Novak et al. [132,133]. It is assumed that the hydrogen trapped at dislocation sites reduces the local stress that impedes dislocation motion and also lowers the reversible work of decohesion (ideal work to fracture) at the tip of dislocation pile-up at the carbide/matrix interface. The HEDE mechanism is modeled as being initiated by a dislocation pile-up against a grain-boundary carbide particle, leading to interface decohesion and intergranular fracture. This assumption is according to the HELP mediated HEDE model for HE [9,106,118]. The model advocates the synergistic action of the HELP and HEDE mechanisms during the intergranular fracture of structural steel. However, our focus

Please cite this article as: Lee HW et al., Modeling fatigue life and hydrogen embrittlement of bcc steel with unified mechanics theory, International Journal of Hydrogen Energy, https://doi.org/10.1016/j.ijhydene.2023.02.110

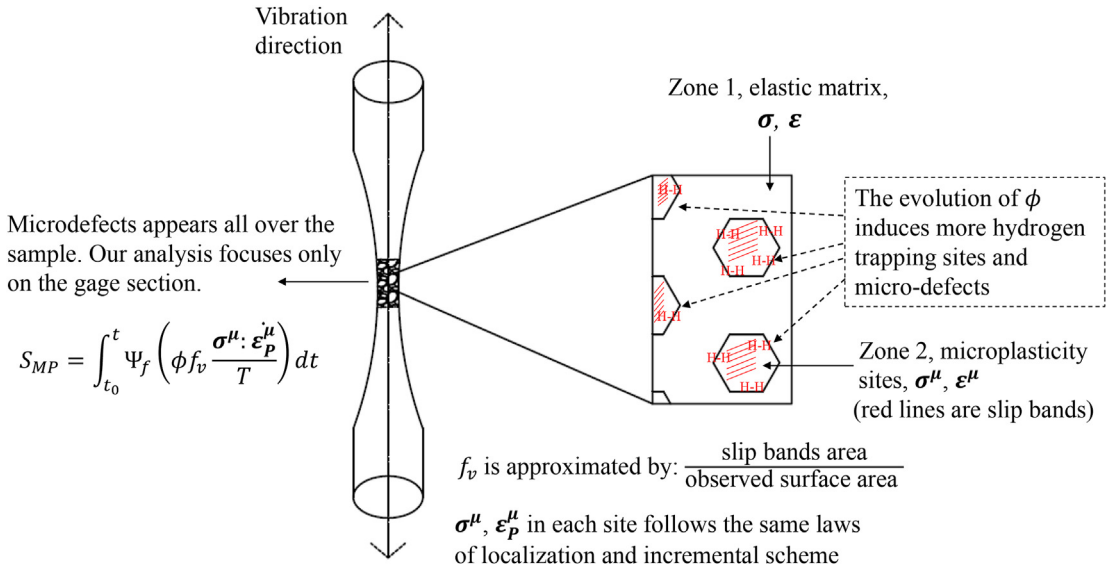

Fig. 3 – Illustration of microplasticity.

is computing the entropy generation due to the activity of the HEDE mechanism rather than predicting cohesive strength decline at the carbide/matrix interface and other hydrogen trapping lattice sites as in the model proposed by Novak et al. [132,133].

The critical strain energy release for decohesion $\mathscr{g}_c$ consists of the ideal work of fracture (energy consumed for fracture/decohesion in the absence of inelastic modes) γ_{int} and the attendant plastic work γ_p accompanying the decohesion event such that $\mathscr{g}_c = 2\gamma_{int} + \gamma_p$. In Hirt and Rice's [134] model, hydrogen is assumed to affect the reversible work of decohesion $2\gamma_{int}$ (also called the ideal work to fracture), as described by Hirth and Rice's [134] thermodynamic theory of decohesion. For the case of fast decohesion [135–138] (i.e., constant hydrogen concentration), the reversible work of decohesion $2\gamma_{int}$ is expressed by Ref. [134]:

$$2\gamma_{int} = (2\gamma_{int})_0 - (\Delta g_i - \Delta g_s)\Gamma = 2\gamma_s - \gamma_i - (\Delta g_i - \Delta g_s)\Gamma \quad (27)$$

where $(2\gamma_{int})_0$ is the ideal work of fracture (decohesion) in the absence of hydrogen, $2\gamma_s$ and γ_i are, the free surface and carbide/matrix interface energies in the absence of hydrogen, respectively and Δg_i and Δg_s are the Gibbs free energy excesses when hydrogen is absorbed into the particle/matrix interface and the free surface created upon separation, respectively. Γ is the interface coverage by hydrogen measured in hydrogen solute atoms per unit area, expressed as $\Gamma = \chi\theta_T^{(d)}\Gamma_{max}$, in which χ is the ratio of impinging dislocation pileup that participates in fracture, $\theta_T^{(d)}$ is the hydrogen occupancy rate in dislocation trapping sites, and Γ_{max} is the maximum number of surface trapping sites, measured in trapping sites per unit area of the carbide/matrix interface.

From equation (27), hydrogen absorption at carbide/matrix interfaces reduces the ideal work of decohesion. In studies of intergranular fracture energy and brittle crack propagation, McMahon and Vitek [139] concluded that the γ_p is proportional to the $2\gamma_{int}$, Jokl et al. [140] established a nonlinear relation between γ_p and $2\gamma_{int}$ based on the concurrent process of atomic bond stretching and breaking during the brittle crack propagation and the dislocation emission from the crack tip. To simplify the relation, Novak et al. [133,134] proposed the following relation of $\gamma_p = A(2\gamma_{int})^q$, and performed a parametric study to obtain the fitting constants A and q for medium carbon steel. In the study of the effects of hydrogen on fracture, Birnbaum [141] revealed that the energy to form the new surfaces $2\gamma_{int}$ is only about 10% of the total fracture energy $\mathscr{g}_c$, with the remainder being the plastic work done during fracture γ_p. This ratio matches the numerical results from Refs. [133,139,140]. Based on these findings in the literature, we use the following relation for the quantitative estimation of γ_p

$$\gamma_p = A(2\gamma_{int})^q = 9(2\gamma_{int})^1 = 0.9\mathscr{g}_c \quad (28)$$

It should be emphasized that $2\gamma_{int}$ and γ_p are material properties independent of crack geometry, loading configuration, etc., as pointed out in Ref. [140]. The decohesion parameters are presented in Table 2, Hydrogen enhanced decohesion model parameters. Based on the data in Table 2, γ_p can be determined to be 28 J/m^2 as the initial value.

It is shown in equation (28) that the irreversible work responsible for the decohesion can be deduced from the reversible work expressed in equation (27). In the condition that the hydrogen concentration in the sample is above the critical value, such that the HEDE mechanism takes place and becomes prevalent, we assume that the HELP and HEDE mechanisms happen simultaneously (HELP + HEDE) at the same defect sites [137]. It should be emphasized that in this study, the microplastic region is around defect sites (i.e., vacancies, inclusions, dislocations cross-slips, or hydrogen solute atoms) instead of an existing notch because there is no initial notch in our specimen (smooth specimen), see Fig. 3. Also, the stress in the microplastic region is below the macroscopic yield stress. Fig. 4 shows the illustration for the formation of the microplasticity region (stage I) and hydrogen-enhanced microplasticity [74–76] and hydrogen-enhanced

Please cite this article as: Lee HW et al., Modeling fatigue life and hydrogen embrittlement of bcc steel with unified mechanics theory, International Journal of Hydrogen Energy, https://doi.org/10.1016/j.ijhydene.2023.02.110

decohesion - HELP + HEDE model [9,11,26,39,78,104,128] (stage II) during very high cycle fatigue.

For the computation of HEDE entropy production ΔS_{hede}, we assume the decohesion happens at defect sites [132,133], Fig. 5. According to HELP mediated HEDE model for HE [106,118], hydrogen facilitates dislocation movements due to the HELP mechanism and leads to high-density dislocation pile-up [132,133,135]. As a result of hydrogen-enhanced dislocation movement, the hydrogen trapped and transported by dislocations increases hydrogen concentration at the carbide [132,133], as shown in Fig. 5, grain boundary [135] and other defect sites acting as dislocation barriers, leading to the interface decohesion due to HEDE activation [9–11,26,104], see Figs. 4 and 5. Therefore, the synergistic effect of HELP and HEDE mechanisms leads to the brittle hydrogen-assisted fracture and microstructural evolution under intergranular fracture [9–11,26,39,104,106,118,132,133,135]. If the plastic work γ_p included in the decohesion process is calculated, then the decohesion entropy generation ΔS_{hede} is given by the following relation,

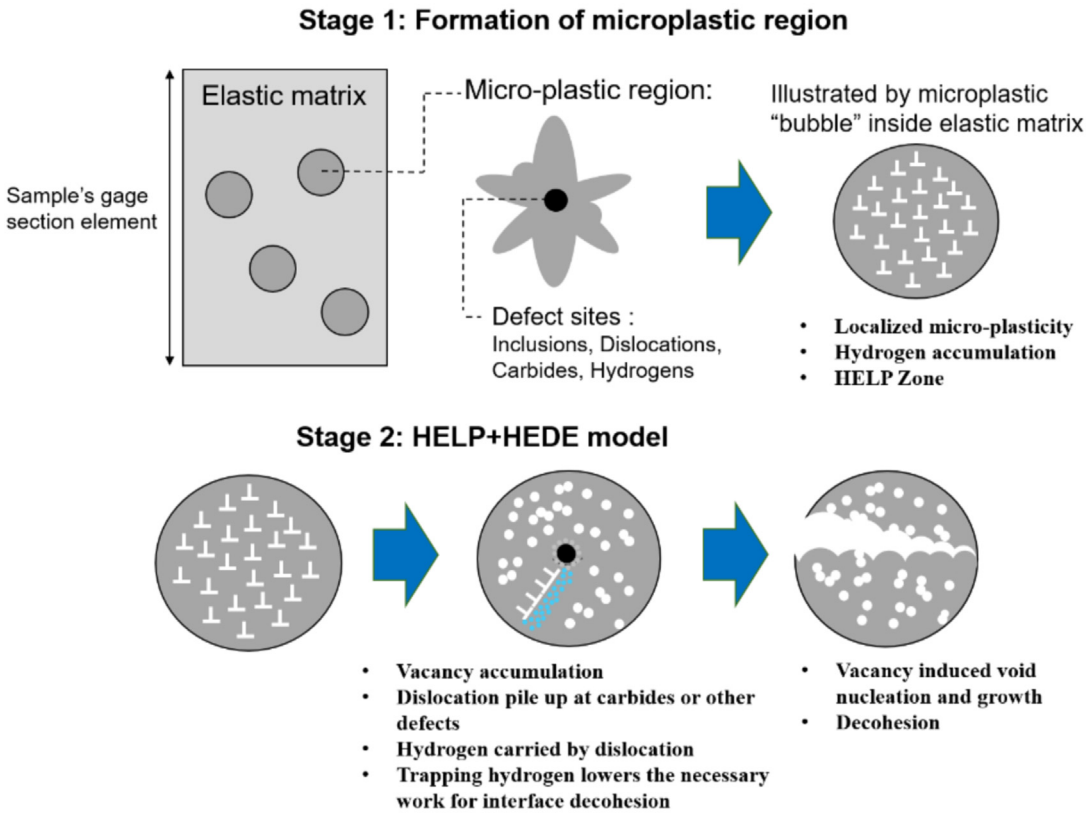

Fig. 4 – Illustration of the HEL(M)P and HEDE model during very high cycle fatigue.

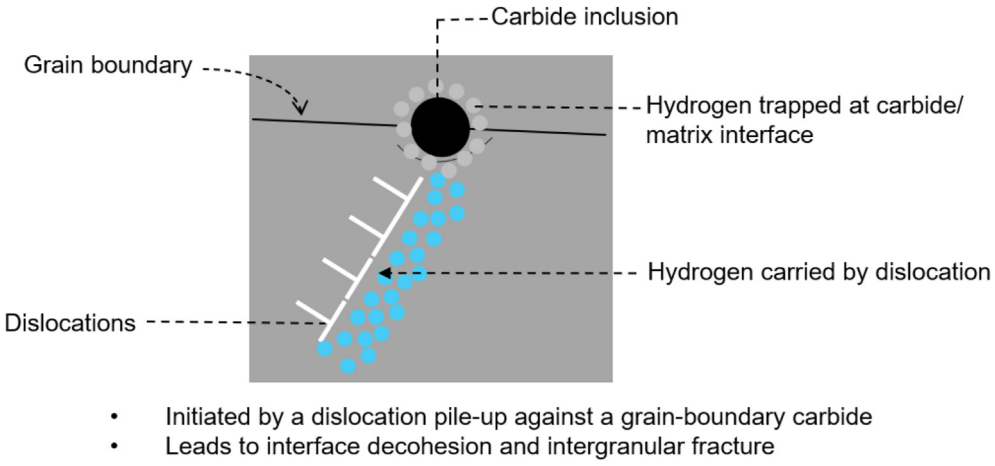

Fig. 5 – Illustration of the HEDE interaction between hydrogen and dislocation, adapted from Refs. [132,133,137].

Please cite this article as: Lee HW et al., Modeling fatigue life and hydrogen embrittlement of bcc steel with unified mechanics theory, International Journal of Hydrogen Energy, https://doi.org/10.1016/j.ijhydene.2023.02.110

$$\Delta S_{hede} = \int_{t_0}^{t} \Phi f_v h_{a/v} \frac{\dot{\gamma}_p}{T} dt \tag{29}$$

where Φ is the TSI, f_v is the volume fraction of activated microdefects, $\dot{\gamma}_p$ is the plastic work of the decohesion process per unit of time, T is the absolute temperature, and $h_{a/v}$ is the surface area to volume ratio, used to convert the entropy unit from J/(K·m^2) to J/(K·m^3). Assuming the carbide particles that result in decohesion at a carbide/matrix interface are all spherical, $h_{a/v} = 4.84$.

Based on equations (27) and (28), the entropy generation due to HEDE in equation (29) is a function of the hydrogen occupancy rate, $\theta_T^{(d)}$, in dislocation trapping sites (equation (29a)), because

$$\gamma_p = A\left[2\gamma_s - \gamma_i - (\Delta g_i - \Delta g_s)\,\eta\,\theta_T^{(d)}\Gamma_{max}\right]^q \tag{29a}$$

All the other parameters are constants. $\theta_T^{(d)}$, and hydrogen occupancy at dislocations is related to the trapped-hydrogen concentration, $C_T^{(d)}$, at dislocations by the relation $C_T^{(d)} = \theta_T^{(d)}\alpha^{(d)}N_T^{(d)}$, which will be discussed later in subsection, Entropy generation due to hydrogen transport, ΔSht. Therefore, the HEDE hydrogen entropy generation rate grows when trapped hydrogen concentration C_T increases.

Entropy generation due to hydrogen-induced dilatation, ΔS_{dl}. A portion of the work of the hydrogen-induced dilatation is irreversible. Because the dilatation caused by the interstitial atom is reversed when the hydrogen atom diffuses out and the lattice returns to its original structure. The entropy production due to this source is calculated based on the product of the stress tensor and the dilatation strain tensor, as follows,

$$\Delta S_{dl} = \left[\int_{t_0}^{t} \frac{\boldsymbol{\sigma} : \dot{\boldsymbol{\varepsilon}}^h}{T} dt\right]_{irr} \tag{30}$$

where $\dot{\boldsymbol{\varepsilon}}^h$ is the rate of hydrogen concentration-induced lattice dilation strain.

The dilatational distortion (lattice distortion) resulting from the hydrogen solute atoms is the source of dilatation strain in the host lattice. The dilatation strain is assumed to be isotropic in bulk, positively related to the change of hydrogen concentration in trapping sites multiplied by the atomic volume of the host lattice. The hydrogen-induced dilatation rate $\dot{\boldsymbol{\varepsilon}}^h$ is given by Refs. [132,133,142]:

$$\dot{\boldsymbol{\varepsilon}}^h = \frac{1}{3}\frac{\lambda}{\rho}\frac{d(C_L - C_L^0)}{dt}\boldsymbol{\delta} = \frac{V_H}{3N_A}\frac{d}{dt}(C_L - C_L^0)\boldsymbol{\delta} \tag{31}$$

where λ is the dilatation induced by a hydrogen solute in the host lattice, ρ is the density, C_L is the hydrogen concentration in the lattice site, C_L^0 is the initial lattice concentration of hydrogen in a stress-free lattice, $\boldsymbol{\delta}$ is an identity tensor, V_H is the partial molar volume of hydrogen, and N_A is Avogadro's number.

Entropy generation due to hydrogen transport, ΔS_{ht}. The entropy generation due to hydrogen transport ΔS_{ht} is given by:

$$\Delta S_{ht} = -\int_{t_0}^{t} \frac{\boldsymbol{J}_h \cdot \nabla\mu_h}{T} dt \tag{32}$$

Where $\boldsymbol{J}_h$ is the hydrogen flux, and $\nabla\mu_h$ is the gradient of the chemical potential of the hydrogen solute atoms.

The diffusion of the hydrogen atoms is driven by the chemical potential gradient $\nabla\mu_h$. Utilizing the Onsager relation, based on Einstein's equation of diffusion, the flux of hydrogen mass transport is given by Refs. [132,133,142,143]:

$$\boldsymbol{J}_h = -\frac{DC_L}{k_B T}\nabla\mu_h \tag{33}$$

The chemical potential μ_h of the hydrogen solute atoms is derived from the constitutive equations based on the Coleman-Noll procedure,

$$\mu_h = \frac{1}{1 + \left(\frac{\partial C_T}{\partial C_L}\right)}\left[k_B T\left(\frac{\theta_L}{1-\theta_L}\right) - \frac{\lambda}{\rho}\sigma_H - \frac{2E}{9(1-\nu)}\left(\frac{\lambda}{\rho}\right)^2 (C_L - C_L^0)\right] \tag{34}$$

Where D is the diffusion coefficient for hydrogen transport in steel lattice, k_B the Boltzmann constant, E Young's modulus, ν Poisson's ratio, and θ_L the occupancy rate of normal interstitial lattice sites (NILS). The chemical potential μ_h of hydrogen, solute atoms can also be written in the standard form as follows

$$\mu_h = \mu_h{}^0 + RT\ln\left(\frac{\theta_L}{1-\theta_L}\right) - \overline{V}_H\sigma_H \tag{35}$$

where $\mu_h{}^0$ denotes the chemical potential in the ground state, σ_H is the hydrostatic stress, and $\overline{V}_H$ the partial molar volume of hydrogen in a solid solution ($\overline{V}_H = 2000\ \text{mm}^3/\text{mol}$ for iron-based materials [144]). In equations (34) and (35), it is evident that where the rate of the trapped hydrogen concentration to the lattice hydrogen concentration is significant (i.e., $\partial C_T/\partial C_L$ is large) or where the lattice hydrogen concentration differs significantly from its initial value (i.e., $C_L \gg C_L^0$), the chemical potential will have a large gradient. It was pointed out that such conditions are likely to exist ahead of a crack tip or a notch [132,133]. Based on the modeling results provided in Ref. [132] where the hydrogen diffusion and hydrogen concentration are computed, for a specimen without a notch, as $\partial C_T/\partial C_L \sim 10^{-5}$ and C_L is very close to C_L^0. Therefore, we use equation (35) because there is no initial notch or crack tip in our study sample.

Combining equations (33) and (35), the flux of hydrogen diffusion through normal interstitial lattice sites (NILS), due to the chemical potential gradient, is given by:

$$\boldsymbol{J}_h = -D\left(\nabla C_L + \frac{C_L\overline{V}_H}{RT}\nabla\sigma_H\right) \tag{36}$$

In equations 33–36, C_L is the hydrogen concentration in normal interstitial lattice sites (NILS), and C_T is the hydrogen concentration in trapping sites. They are related to their corresponding occupancies through the following relations $C_L = \theta_L\beta N_L$ and $C_T = \theta_T{}^{(i)}\alpha^{(i)}N_T{}^{(i)}$, where θ_L denotes the occupancy rate of NILS, θ_T is the occupancy rate of the trapping sites, β is the number of lattice sites per solvent atom, and α is the number of trapping sites per trap. The superscript (i) can be (d), (c), and (gb), which represent dislocations, carbides, and grain boundaries, respectively. For bcc metals usually $\alpha = 1$ and $\beta = 6$ [145]. N_L is the density ofthe host metal lattice measured in solvent atoms per unit volume, N_T is the density of traps measured in traps per unit volume

Please cite this article as: Lee HW et al., Modeling fatigue life and hydrogen embrittlement of bcc steel with unified mechanics theory, International Journal of Hydrogen Energy, https://doi.org/10.1016/j.ijhydene.2023.02.110

[132,133,142,143]. Typical lattice and trapping sites for hydrogen in steel are a) NILS (for lattice diffusion); b) surface traps; c) subsurface traps; d) grain and interphase boundaries; e) dislocations traps; and f) vacancies [146,147]. The trapping site and lattice hydrogen populations can be related through Oriani's theory of assuming the fast trapping and un-trapping kinetics, such that the trapped hydrogen concentration is always in equilibrium with the lattice concentration [132,133,142–144],

$$\frac{\theta_T^{(i)}}{1-\theta_T^{(i)}} = \frac{\theta_L}{1-\theta_L}\exp\left(\frac{W_B^{(i)}}{RT}\right) \tag{37}$$

From equation (37), one can derive the following relation:

$$\frac{C_T^{(i)}}{\alpha^{(i)}N_T^{(i)} - C_T^{(i)}} = \frac{C_L}{\beta N_L - C_L}\exp\left(\frac{W_B^{(i)}}{RT}\right) \tag{38}$$

where $W_B^{(i)}$ is the trapping binding energy associated with the trap type (dislocation trap, carbides trap, grain boundary traps, etc), and R is the gas constant. Equation (38) is used to relate the hydrogen concentration in trapping sites C_T to the hydrogen concentration in lattice sites C_L. In the absence of loading (stress-free state), the hydrogen concentration is uniform through NILS. The initial NILS hydrogen concentration is given by Refs. [148–150]:

$$C_L^0 = N_L \exp\left(\frac{T\Delta S_H - \Delta H_H}{RT}\right) \tag{39}$$

where ΔH_H and ΔS_H are the partial formation enthalpy and partial molar excess entropy (formation entropy) of the interstitially dissolved hydrogen. The density of the host metal lattice N_L is a constant number given by $N_L = N_A/V_M$, with N_A being Avogadro's number, and V_M is the molar volume of the host lattice. The hydrogen trapping density N_T is related to the dislocation density using the flow stress. N_T is given by Refs. [132,133]:

$$N_T = N_T^0 + \left(\frac{\kappa}{K_\kappa G}\right)^2 \frac{1}{b^3} = \left(\frac{Y_0}{K_\kappa G}\right)^2 \frac{1}{b^3} + \left(\frac{\kappa}{K_\kappa G}\right)^2 \frac{1}{b^3} \tag{40}$$

Where Y_0 is the initial yield stress, G is the shear modulus, b is the dislocation burger's vector, K_κ is a dimensionless material constant (Taylor's hardening parameter), and κ is the flow stress.

On the other hand, Fernández-Sousa et al. [143] proposed that the hydrogen-trapping density N_T is related to the contribution of dislocations, carbides, and martensite interfaces, given by a summation as $N_T = N_T^{(d)} + N_T^{(c)} + N_T^{(m)}$, in which:

$$N_T^{(d)} = \frac{\sqrt{2}\rho}{a} \tag{41}$$

$$N_T^{(c)} = \left(\sum_j \pi d_j^2 f_j\right)\frac{4}{a^2}\frac{1}{L^3} = \left(\alpha^{(c)}\right)\frac{4}{a^2}\frac{1}{L^3} \tag{42}$$

$$N_T^{(m)} = \frac{b}{D_g}N_L \tag{43}$$

Where a is the lattice parameter, ρ is a function of plastic strain and plastic strain gradient, d is the carbide particle diameter, L is the average distance between the carbide particles, and f is the loading frequency. Based on equations (41–43), it is shown that the hydrogen trapping density at carbides $N_T^{(c)}$, $N_T^{(m)}$ are constants based on the geometry of the trapping sites, whereas hydrogen trapping density at dislocations $N_T^{(d)}$ increases with plastic strain. However, it is important to point out ultrasonic vibration operates in a linear elastic range. Hence, we may assume $N_T^{(d)}$ as constant, and we can obtain its initial value from equation (40).

Using equations (39–43), the initial NILS hydrogen concentration C_L^0 (atoms per unit volume) and the initial trapping density N_T^0 (traps per unit volume) can be estimated. Then, the corresponding C_T^0 can be obtained from equation (38). During the loading, the change in C_L and C_T with time is calculated through the hydrogen mass transport equation, given by:

$$\frac{\partial C_L}{\partial t} + \frac{\partial C_T}{\partial t} = D\nabla^2 C_L + \nabla\left(\frac{DC_L}{RT}\overline{V}_H\nabla\sigma_H\right) \tag{44}$$

Combining equation (44) with Oriani's equilibrium theory, a transient hydrogen transport model that was first derived by Sofronis and McMeeking [151] and later modified by Krom et al. [152] is given in the following form:

$$\frac{C_L + C_T(1-\theta_T)}{C_L}\frac{\partial C_L}{\partial t} = D\nabla^2 C_L + \nabla\left(\frac{DC_L}{RT}\overline{V}_H\nabla\sigma_H\right) - \alpha\theta_T\frac{dN_T}{d\varepsilon_p}\frac{d\varepsilon_p}{dt} \tag{45}$$

Equation (45) accounts for hydrogen trapping by dislocations and hydrostatic drift. The last term is the plastic strain rate factor, accounting for the effect of the plastic strain rate on the transient hydrogen concentrations. The last term disappears in the absence of macroscopic plastic strain.

Equations (32) and (33) show the entropy generation due to lattice hydrogen transportation that promotes hydrogen embrittlement, while equations (44) and (45) govern the transportation. However, it is well understood that in principle, quantum tunneling [153–156] can also contribute to H's high diffusivity in bcc Fe besides classical diffusion [153–155]. Quantum tunneling allows the hydrogen atoms to move through barriers they could not move through in classical mechanics, which can be the dominant mechanism for H diffusion in metals at low temperatures (e.g., T < 10K for V, Nb, and Ta) [155]. Nevertheless, we do not consider quantum tunneling diffusion in our model because 1) ultrasonic vibration fatigue generates high temperature (up to 440K at failure), and 2) we aim to establish our model in classical continuum mechanics which satisfies equilibrium thermodynamics. For quantum mechanics, we may have to apply statistical thermodynamics, which is out beyond the scope of the current work.

Entropy generation due to coupling source, ΔS_{coup}. The entropy generation due to the coupling of plastic strain with transient hydrogen concentrations is given by the following relation [132,133]:

$$\Delta S_{coup} = \int_{t_0}^{t} \frac{(\gamma_b + \mu_h)\alpha\theta_T}{T}\frac{\partial N_T}{\partial \varepsilon^p}\dot{\varepsilon}^p dt \tag{46}$$

where γ_b is the microforce resulting from the lattice dilation due to hydrogen solute atoms, μ_h is the chemical potential, α is the number of trapping sites per trap, θ_T is the occupancy rate of the hydrogen trapping sites, and N_T is the density of traps measured in traps per unit volume.

Please cite this article as: Lee HW et al., Modeling fatigue life and hydrogen embrittlement of bcc steel with unified mechanics theory, International Journal of Hydrogen Energy, https://doi.org/10.1016/j.ijhydene.2023.02.110

$$\Delta S_{coup} = \int_{t_0}^{t} \left[RT \ln\left(\frac{\theta_L}{1-\theta_L}\right) - \overline{V}_H \sigma_H \right] \frac{\alpha\theta_T}{T} \frac{\partial N_T}{\partial \varepsilon^p} \dot{\varepsilon}^p dt \quad (47)$$

Using the transient hydrogen transport equation, the $\alpha\theta_T \frac{\partial N_T}{\partial \varepsilon^p}\dot{\varepsilon}^p$ is equivalent to:

$$\alpha\theta_T \frac{dN_T}{d\varepsilon_p}\frac{d\varepsilon_p}{dt} = -\nabla\cdot(J_h) - \left[1+\frac{\partial C_T}{\partial C_L}\right]\dot{C}_L \quad (48)$$

Finally, we have:

$$\Delta S_{coup} = \int_{t_0}^{t} \frac{1}{T}\left[RT \ln\left(\frac{\theta_L}{1-\theta_L}\right) - \overline{V}_H \sigma_H \right]\left[-\nabla\cdot(J_h) - \left[1+\frac{\partial C_T}{\partial C_L}\right]\dot{C}_L \right] dt \quad (49)$$

It should be noted that equations (46) and (49) compute entropy generation due to coupling between hydrogen trapping sites and macroscopic plastic strain. This coupling source can be ignored in the case of ultrasonic vibration fatigue where macroscopic plastic strain is zero.

Thermodynamic fundamental equation for steel pre-charged with H and then subjected to ultrasonic vibration fatigue, ΔS

Combining all entropy production mechanisms, the total specific entropy production can be expressed by the following relation:

$$\begin{aligned}\Delta s = & \int_{t_0}^{t} \frac{1}{\rho T}\left(J_{M,a}\alpha_M z_M F\eta + J_{M,c}(1-\alpha_M) z_M F\eta + J_{O,a}\alpha_o z_O F\eta + J_{O,c}(1\right. \\ & \left. -\alpha_O) z_O F\eta\right) dt_{corr} + \int_{t_0}^{t} \frac{k_h}{\rho T^2}(\nabla T\cdot\nabla T)dt \\ & + \int_{t_0}^{t} \frac{\left(\varrho B^{drag} v^2 + \frac{1}{2}Gb^2\dot{\varrho} - \alpha_H Gb\sqrt{\varrho}\,\dot{\gamma}\right)}{\rho T} dt \\ & + \int_{t_0}^{t} \Psi_f\left(\Phi f_v \frac{\boldsymbol{\sigma}^{\mu}:\dot{\boldsymbol{\varepsilon}}_p^{\mu}}{\rho T}\right) dt + \int_{t_0}^{t} \Phi f_v h_{a/v}\frac{\dot{\gamma}_p}{\rho T} dt + \int_{t_0}^{t} \frac{\boldsymbol{\sigma}:\dot{\boldsymbol{\varepsilon}}^h}{\rho T} dt \\ & - \int_{t_0}^{t} \frac{J_h\cdot\nabla\mu_h}{\rho T} dt + \int_{t_0}^{t} \frac{(\gamma_b+\mu_h)\alpha\theta_T}{\rho T}\frac{\partial N_T}{\partial\varepsilon^p}\dot{\varepsilon}^p dt\end{aligned} \quad (50)$$

By calculating the cumulative specific entropy production using equation (50) and inserting it into the TSI (equation (3)), the TSI coordinate which can be between 0 and near 1 (or Φ_{cr}), can be computed. Table 1 summarizes the entropy equations derived in this section and the assumptions used to compute them in the following sections.

It is shown in Table 1 that to compute each entropy generation term, many intrinsic parameters need to be determined. However, many of them do not affect the sensitivity of the total entropy production because, through the order of magnitude analysis, some entropy generation terms are negligible compared to others. It will be shown at the end of section Entropy generation order of magnitude comparison that only ΔS_{corr}, ΔS_t, ΔS_r, ΔS_{mp}, and ΔS_{hede} affects the final results. The preciseness of these five terms is determined by the results of the Tafel test electrochemical parameters, the temperature measured on the sample, the dislocation parameters related to phonon dragging, the hydrogen-dependent parameters in the microplasticity model, and the trapping hydrogen concentration in the decohesion model, respectively. Among them, the Tafel constants and temperature can be most straightforwardly measured from the test. The hydrogen-dependent parameters can also be calibrated through simple mechanical testing on hydrogen-charged samples. Whereas the dislocation parameters and trapping hydrogen concentration are strongly affected by the microstructure of the material.

The model parameters used in this study are collected and listed in Table 2.

Entropy generation order of magnitude comparison

In this section, several numerical simulations were performed to compare the order of magnitude of the entropy generation mechanisms presented and discussed in section Thermodynamic fundamental equation.

Calculation of entropy production due to corrosion in the H_2SO_4 *solution*

The calculation of entropy production due to corrosion using equation (8) requires the determination of electrochemical parameters (such as E_{corr}, I_{corr}, α_a, and α_c) based on Tafel plots. Our recent study about corrosion fatigue [76] validated the corrosion entropy production for 40 days of immersion time in 5 wt% NaCl solution to be around 0.2 on the TSI axis. The Tafel test was not repeated in this study because the variation of electrochemical parameters obtained from Tafel tests at different stages of corrosion has a negligible contribution to the overall TSI evolution.

The electrochemical polarization parameters required for calculating corrosion entropy production are presented in Table 2, Electrochemical parameters, for low carbon steel in 1 M H_2SO_4 solution, based on the data from Ref. [90], which has a similar chemical composition to the sample used in our study and an identical corrosion media concentration. When hydrogen charging is conducted by immersing samples in an H_2SO_4 solution without applying a constant electrode overpotential, the anodic flux for metal dissolution $J_{M,a}$ and the cathodic flux for the evolution of hydrogen $J_{O,c}$ should be both equivalent to the corrosion current I_{corr}, according to the mixed potential theory [85]. In this special case, the driving force is the potential difference ΔE between the oxidized (or reduced) species. Therefore, the entropy generation ΔS_{act} is merely due to ΔE and I_{corr},

$$\Delta S_{act} = \frac{1}{T}\int_{t_0}^{t}\left(J_{M,a}\Delta E + J_{O,c}\Delta E\right)dt_{corr} = \frac{1}{T}\int_{t_0}^{t}\left[I_{corr}\left(E^0_{H^2} - E^0_{Fe^{2+}}\right)\right]dt_{corr} \quad (51)$$

where $E^0_{H^2}$ is the standard hydrogen electrode potential, which is set to 0V. The standard cell overpotential for the dissolution of iron $Fe \leftrightarrow Fe^{2+} + 2e^-$ and the evolution is $E^0_{Fe^{2+}} = -0.440$ V [157].

The simulated cumulative entropy production versus corrosion time based on equation (51) is shown in Fig. 6. It shows a linear relation between corrosion entropy production and corrosion time for samples in 1 M H_2SO_4 solution because we assume that the electrochemical material properties are

Table 1 – Summarization of thermodynamic fundamental equations.

Entropy equation	Important Parameters	Assumptions
$\Delta S_{corr} = \int \frac{1}{T}(J_{M,a}\alpha_M z_M F\eta + J_{M,c}(1-\alpha_M)z_M F\eta + J_{O,a}\alpha_o z_O F\eta + J_{O,c}(1-\alpha_O)z_O F\eta)dt_{corr}$	$J_{M,a} = j_{0,M}\left[\exp\left(\frac{\alpha_{M,a}\tilde{A}_M}{RT}\right)-1\right]$ $J_{M,c} = -j_{0,M}\left[\exp\left(\frac{-\alpha_{M,c}\tilde{A}_M}{RT}\right)-1\right]$ $J_{O,a} = j_{0,R}\left[\exp\left(\frac{\alpha_{O,a}\tilde{A}_O}{RT}\right)-1\right]$ $J_{O,c} = -j_{0,R}\left[\exp\left(\frac{-\alpha_{O,c}\tilde{A}_O}{RT}\right)-1\right]$	Use $j_{0,M}$, $j_{0,R}$ value from references. $\alpha_{M,a}$, $\alpha_{M,c}$, $\alpha_{O,c}$, $\alpha_{O,c}$ can be measured from tests or use data from reference as a first approximation.
$\Delta S_t = \int_{t_0}^{t}\frac{k_h}{T^2}(\nabla T\cdot\nabla T)dt$	k_h, ∇T	Assume a one-dimensional conduction path from the gauge to the grip section.
$\Delta S_r = \int_{t_0}^{t}\frac{(\varrho B^{drag}v^2)}{T}dt + \int_{t_0}^{t}\frac{\left(\frac{1}{2}Gb^2\dot{\varrho} - \alpha_H Gb\sqrt{\varrho}\,\dot{\gamma}\right)}{T}dt$	Dislocation parameters such as μ, b, ϱ, and α_H …	The parameters may be obtained from discrete dislocation dynamic (DDD) simulations. We use the data from reference [75].
$\Delta S_{mp} = \int_{t_0}^{t}\Psi_f\left(\Phi f_v\frac{\boldsymbol{\sigma}^{\mu}:\dot{\boldsymbol{\varepsilon}}_P^{\mu}}{T}\right)dt$	$\boldsymbol{\sigma}^{\mu} = \boldsymbol{\sigma} - \left[\frac{E(5\nu-7)}{15(\nu^2-1)}\right](1-f_v)\boldsymbol{\varepsilon}_P^{\mu}$ $\dot{\boldsymbol{\varepsilon}}_P^{\mu} = \dot{\varepsilon}_0\sinh\left[\tilde{\Psi}\left(\frac{\sigma_e^{\mu}}{\tilde{y}+\kappa^{\mu}}-1\right)^n\right]\frac{\boldsymbol{\sigma}^{\mu\prime}}{\sigma_e^{\mu}}$	$\tilde{\Psi}(C) = \Psi_0\left(1+\Psi_c\frac{C_T}{C_0}\right)$; $\tilde{y}(C) = y_0\left(1+y_c\frac{C_T}{C_0}\right)$; $\tilde{H}(C) = H_0\left(1+H_c\frac{C_T}{C_0}\right)$
$\Delta S_{hede} = \int_{t_0}^{t}\left(\Phi f_v h_{a/v}\frac{\dot{\gamma}_p}{T}\right)dt$	$\gamma_p = A[2\gamma_s-\gamma_i-(\Delta g_i-\Delta g_s)\eta\theta_T^{(d)}\Gamma_{max}]^q$ Φ, $\theta_T^{(d)}$ are the only two variables. Φ is the TSI, $\theta_T^{(d)}$ is the trapping H occupancy at dislocations related to C_T: $\theta_T^{(d)}\alpha^{(d)}N_T^{(d)} = C_T^{(d)}$	$\alpha^{(d)} = 1$ $N_T^{(d)} = \frac{\rho_{ss}}{b}$ is related to the SSDs. Assume $N_T^{(d)}$ is equivalent to the initial value $N_{T0}^{(d)} = \left(\frac{Y_0}{K_\kappa G}\right)^2\frac{1}{b^3}$ $N_T^{(d)}$ is constant because the fatigue loading is in the linear elastic range.
$\Delta S_{dl} = \left[\int_{t_0}^{t}\frac{\boldsymbol{\sigma}:\dot{\boldsymbol{\varepsilon}}^h}{T}dt\right]_{irr}$	$\dot{\boldsymbol{\varepsilon}}^h = \frac{1}{3}\frac{\lambda}{\rho}\frac{d(C_L-C_L^0)}{dt}\boldsymbol{\delta}$ $= \frac{V_H}{3N_A}\frac{d}{dt}(C_L-C_L^0)\boldsymbol{\delta}$	Assume 5% is irreversible.
$\Delta S_{ht} = -\int_{t_0}^{t}\frac{\boldsymbol{J_h}\cdot\nabla\mu_h}{T}dt$	$\boldsymbol{J_h} = -\frac{DC_L}{k_B T}\nabla\mu_h$ $= -D\left(\nabla C_L + \frac{C_L\overline{V}_H}{RT}\nabla\sigma_H\right)$	Assume a constant H lattice concentration gradient and a one-dimensional diffusion path (proposed boundary conditions).
$\Delta S_{coup} = \int_{t_0}^{t}\frac{(\gamma_b+\mu_h)\alpha\theta_T}{T}\frac{\partial N_T}{\partial\varepsilon^p}\dot{\varepsilon}^p dt$	θ_T, N_T, $\dot{\varepsilon}^p$ …	$\frac{\partial N_T}{\partial\varepsilon^p} = 0$ because no macroplastic strain.

Please cite this article as: Lee HW et al., Modeling fatigue life and hydrogen embrittlement of bcc steel with unified mechanics theory, International Journal of Hydrogen Energy, https://doi.org/10.1016/j.ijhydene.2023.02.110

Table 2 – Model parameters.

Electrochemical parameters for low carbon steel in 1M H_2SO_4 solution [91]. For corrosion entropy computation

E_{corr} (mV)	I_{corr} (μ A/cm^2)	β_c (mV/dec)	β_a (mV/dec)	α_c	α_a
−441	342.22	99	76.7	0.607	0.39

Material parameters of steel sample (S355J2 + N, equivalent to ASTM A656) [75]. For heat conduction and microplasticity computation

Young's modulus, E	197265 MPa	Macroscopic yield stress, σ_y	400 MPa
Hardening coefficient, H_0	879 MPa	Microscopic yield stress, σ_y^μ	368 ± 3.3 MPa
Poisson's ratio, ν	0.27	Thermal expansion coefficient, α	$12.6\cdot10^{-6}$ K^{-1}
Density, ρ	7820 kg m^{-3}	Specific heat capacity, c_V	470 J kg^{-1}K^{-1}
The volume fraction of activated defect sites, f_v	20%	Thermal conductivity, k_h	50 WK^{-1}m^{-1}
Critical thermodynamic index, Φ_{cr}	0.97	Frequency coefficient, Ψ_f	$5\cdot10^{-3}$

Hydrogen enhanced microplastic strain rate function parameters for equations (24–26). For HEL(M)P entropy computation

n	Ψ_0	y_0	H_0	Ψ_c	y_c	H_c
2	0.105	368 MPa	879 MPa	10.5	0.1	0

$C_T = 0$ (reference)	$\tilde{\Psi} = 0.105$, $\tilde{H} = 879$ MPa, $\tilde{y} = 3\ 54$ MPa
$C_T = 0.25C_0$	$\tilde{\Psi} = 0.328$, $\tilde{H} = 879$ MPa, $\tilde{y} = 362$ MPa
$C_T = 0.5C_0$	$\tilde{\Psi} = 0.551$, $\tilde{H} = 879$ MPa, $\tilde{y} = 371$ MPa

Hydrogen-enhanced decohesion model parameters [133,140]. **For HEDE entropy computation**

γ_s (J/m^2)	γ_i (J/m^2)	Δg_i (kJ/mol)	Δg_s (kJ/mol)	Γ_{max}	χ
1.95	0.78	−100	−25.5	6.17×10^{24}	0.01

Hydrogen concentration and diffusion coefficients [132,133,144,148–150,159]. **For other hydrogen term computation**

Avogadro's number N_A	6×10^{23} mol^{-1}	Gas constant R	8.31 J·mol^{-1}K^{-1}
Diffusion coefficient, D	$3.53 \times 10^{-3}\exp(\frac{-12600}{RT})$ m^2/s	Boltzmann's constant, k_B	$1.38\cdot10^{-23}$ J·K^{-1}
The molar volume of the host lattice, V_M	6.98×10^{-6} m^{3}mol^{-1}	Partial molar volume of hydrogen in solid solution, $\overline{V}_H$	2000 mm^3/mol
Partial molar enthalpy for the formation of interstitially dissolved hydrogen, ΔH_H	57.9 kJ/mol	Partial molar entropy for the formation of interstitially dissolved hydrogen, ΔS_H	− 4.157 J·mol^{-1}K^{-1}
Dislocation trap binding energy, $W_B^{(d)}$	25 kJ/mol	Dislocation burgers vector, b	0.258 nm

constant throughout the process. In comparison, the results of samples corroded in 5 wt% NaCl solution, based on [76], shows a nonlinear relation. The difference between the two relations is because electrochemical material properties used for the calculation of NaCl corrosion entropy production were measured at different stages during corrosion experiments, which vary depending on immersion/corrosion time. However, our assumption for H_2SO_4 corrosion entropy production is still valid and sufficient for all parametric study purposes because we are overestimating the entropy generation by using a linear function. The actual value will be lower if the actual electrochemical material properties are measured during the H_2SO_4 corrosion experiment. For a 4-week hydrogen charging (corrosion) in 1 M H_2SO_4 solution, the entropy generation is around 0.25 MJK^{-1}m^{-3}.

Calculation of entropy production due to mechanical loading

The entropy generation due to mechanical loading consists of thermal conduction, internal friction, and microplasticity. In detail, the dislocation parameters for internal friction entropy production are discussed in Ref. [75]. Computation of thermal conduction and microplasticity entropy production requires basic material constants. They are presented in Table 2, Material parameters of steel sample. The entropy generation due to mechanical loading is shown in Fig. 9.

Calculation of entropy production due to hydrogen-enhanced mechanisms

The entropy generations due to HEDE, and hydrogen lattice dilatation can be directly computed utilizing the data in Table 2. Therefore, the focus of this section is HEL(M)P and hydrogen transport.

Hydrogen-enhanced microplasticity entropy production

In the presence of hydrogen, the microplastic strain increment in the microplastic model is enhanced based on equation (22). The parameters for modeling hydrogen concentration-dependent functions are given in Table 2, Hydrogen enhanced microplastic strain rate function parameters. In Table 2, Hydrogen enhanced microplastic strain rate function parameters, the material parameters n and Ψ_0 were calculated by fitting the microplastic stress-strain curve from equation (19) to equation (22) without hydrogen participation. The y_0 and H_0 are simply the microscopic yield stress (fatigue

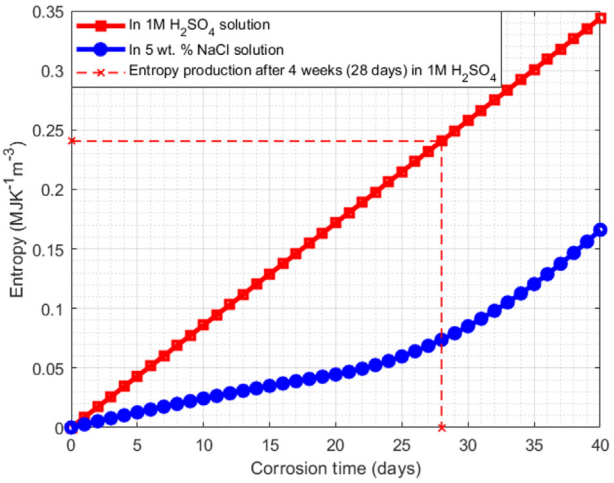

Fig. 6 – Corrosion entropy production versus corrosion time for samples corroded in a different solution.

limit) and hardening modulus of the sample measured before the hydrogen test. Ψ_c, y_c, H_c are positive dimensionless parameters discussed in the following section:

a. Novak et al. [132] experimentally studied four different types of steel and concluded that hydrogen concentration has a negligible effect on the hardening modulus. Therefore, $H_c = 0$.
b. For a hydrogen pre-charged low carbon ferrite steel, the yield stress increases slightly depending on the hydrogen charging time and the resulting hydrogen concentration but eventually reaches a steady state [158]. Based on the literature, we assume a 10% increase in yield stress after sufficient hydrogen charging. Then, we obtain $y_c = 0.1$ based on equation (25).
c. According to equations (22) and (24), the hydrogen-induced softening parameter, Ψ_c, determines the micro-plastic strain enhancement due to hydrogen concentration. Ψ_c can be determined utilizing the stress-strain curve of the hydrogen-charged sample. A value of 10.5 was obtained from the stress-strain curve.

Fig. 7 shows the hydrogen-enhanced microplastic hysteresis loop based on equation (22) for different values of dislocation motion activation energy parameter $\tilde{\Psi}$, under the ultrasonic vibration at 400 MPa stress amplitude. The entropy production for HEL(M)P is estimated by the amount of energy dissipated by hysteresis loops.

Hydrogen transport entropy production

The calculation of this term requires parameters related to the hydrogen concentration and diffusion, as well as proper boundary conditions. They are given in Table 2, Hydrogen concentration and diffusion coefficients, and Fig. 8.

As shown in Fig. 8, the sample is subjected to ultrasonic vibration resulting in a 400 MPa normal stress at the gage center. The measured temperature at the gage section of the steel sample rises from 300K to 400K before the initiation of macrocracks [73]. In contrast, the measured temperature at the grip section remains relatively steady. The temperature varies parabolically along the sample's centerline [along the height] from gage to grip, a simple one-dimensional thermal gradient ∇T that increases as the temperature at the gage center rises. This temperature gradient ∇T is also used for the thermal conduction entropy production in subsection Entropy generation due to thermal conduction, ΔSt.

No hydrogen gas pressure was applied during the vibration test. Therefore, the hydrogen in the lattice sites (diffusible hydrogen) will outgas to the atmosphere as the temperature increases. For the calculation of hydrogen flux J_h, in equation (36) the diffusion coefficient D, the gradient of the concentration of the hydrogen solute atoms residing in normal interstitial lattice sites (NILS) ∇C_L, the partial molar volume of hydrogen in a solid solution $\overline{V}_H$, and the gradient of the hydrostatic stress $\nabla\sigma_H$ are required.

For simplicity and the purpose of numerical comparison, we made several simple assumptions (as shown in Fig. 8).

a. A one-dimensional diffusion path from the center of the gage to the atmosphere ($d = 4$ mm).
b. C_L at the surface is 0.
c. The elevated temperature is constant at 400K.
d. The vibration stress amplitude is 400 MPa.

Therefore, we can estimate the entropy production as follows:

The hydrogen transport in this study is controlled by lattice diffusion, as suggested in Refs. [132,133,155,160]. The lattice hydrogen diffusion coefficient D for low carbon steel is given by Ref. [160]:

$$D = 3.53\times10^{-3}\exp\left(\frac{-12600}{RT}\right) \approx 8\cdot10^{-5}m^2s^{-1} \quad (52)$$

at elevated temperature, $T = 400$K during ultrasonic fatigue.

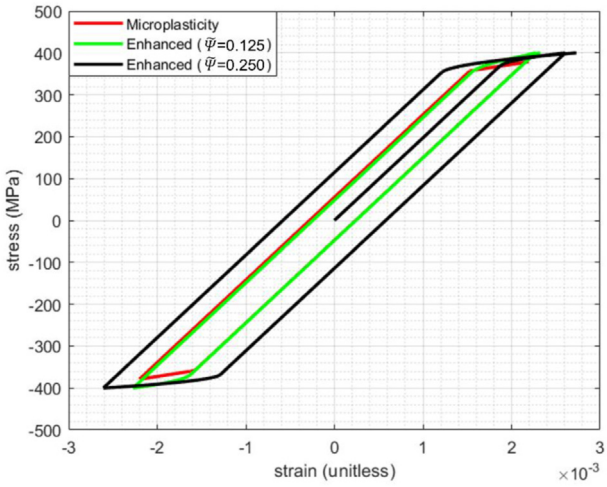

Fig. 7 – Hydrogen-enhanced microplastic hysteresis loops for different values of dislocation motion activation energy $\tilde{\Psi}$.

Please cite this article as: Lee HW et al., Modeling fatigue life and hydrogen embrittlement of bcc steel with unified mechanics theory, International Journal of Hydrogen Energy, https://doi.org/10.1016/j.ijhydene.2023.02.110

The initial concentration of the hydrogen solute atoms residing in NILS, C_L^0, can be calculated using equation (39), where the partial molar enthalpy for the interstitial lattice site formation ΔH, the partial molar entropy of solution ΔS, and the gas constant R are presented in Table 2, Hydrogen concentration and diffusion coefficients. N_L is the density of the host metal lattice measured in solvent atoms per unit volume, which is a constant given by:

$$N_L = N_A/V_M = 8.6 \times 10^{28} \text{atoms} \cdot \text{m}^{-3} \tag{53}$$

Hence, the initial uniform hydrogen concentration in NILS at a stress-free state C_L^0 is

$$C_L^0 = N_L \exp\left(\frac{T\Delta S_H - \Delta H_H}{RT}\right) = 6.685 \times 10^{19} \text{H atoms} \cdot \text{m}^{-3} \tag{54}$$

The corresponding initial hydrogen concentration in trapping sites C_T^0 can be obtained by using the following relation:

$$C_T^0 \cong \alpha N_T^0 \frac{C_L}{\beta N_L - C_L} \exp\left(\frac{W_B}{RT}\right) = 3.7 \times 10^{17} \text{ H atoms} \cdot \text{m}^{-3} \tag{55}$$

The total initial hydrogen concentration C_0 is given by:

$$C_0 = C_L^0 + C_T^0 = 6.72 \times 10^{19} \text{ H atoms} \cdot \text{m}^{-3} \tag{56}$$

Hence, the hydrogen flux J_h can be calculated by the following relation:

$$J_h = -D\left(\nabla C_L + \frac{C_L \overline{V}_H}{RT} \nabla \sigma_H\right) = -2.665 \cdot 10^{18} \text{H atoms} \cdot \text{m}^{-2}\text{s}^{-1} \tag{57}$$

Finally, the entropy production of the hydrogen transport ΔS_{HT} can be obtained by equation (58):

$$\Delta S_{ht} = -\int_{t_0}^{t} \frac{J_h \cdot \nabla \mu_h}{T} dt = \int_{t_0}^{t} \frac{k_B T}{D C_L} \left(\frac{J_h \cdot J_h}{T}\right) dt = 0.0184 \frac{J}{K \cdot m^3 \cdot s} \cdot \Delta t \tag{58}$$

For a test duration of 1 hour, the entropy production of the hydrogen transport is:

$$\Delta S_{ht} = 66.24 \frac{J}{K \cdot m^3} \tag{59}$$

This magnitude of entropy is very small compared to the entropy production due to microplasticity, which is usually in the order of $\frac{MJ}{K \cdot m^3}$. Therefore, it will have a trivial effect.

We should emphasize that hydrogen concentration used in calculations should be a function of temperature. The trapped hydrogen concentration will be re-distributed due to the mechanical energy input to the sample through ultrasonic vibration. However, the purpose of this study is the derivation of the thermodynamic fundamental equations and to compare the order of magnitude of different entropy generation mechanisms.

Summary: order of magnitude comparison

The entropy generation due to mechanical loading and hydrogen-enhanced mechanisms is calculated. Fig. 9 (a) and (b), and Table 3 compare their order of magnitude. Fig. 9 (c) gives the percentage of the entropy contribution from each mechanism for different vibration stress amplitudes.

It is shown that the hydrogen transport and lattice dilatation entropy generations are negligible compared to the other mechanisms. The HEL(M)P dominates the entropy generation

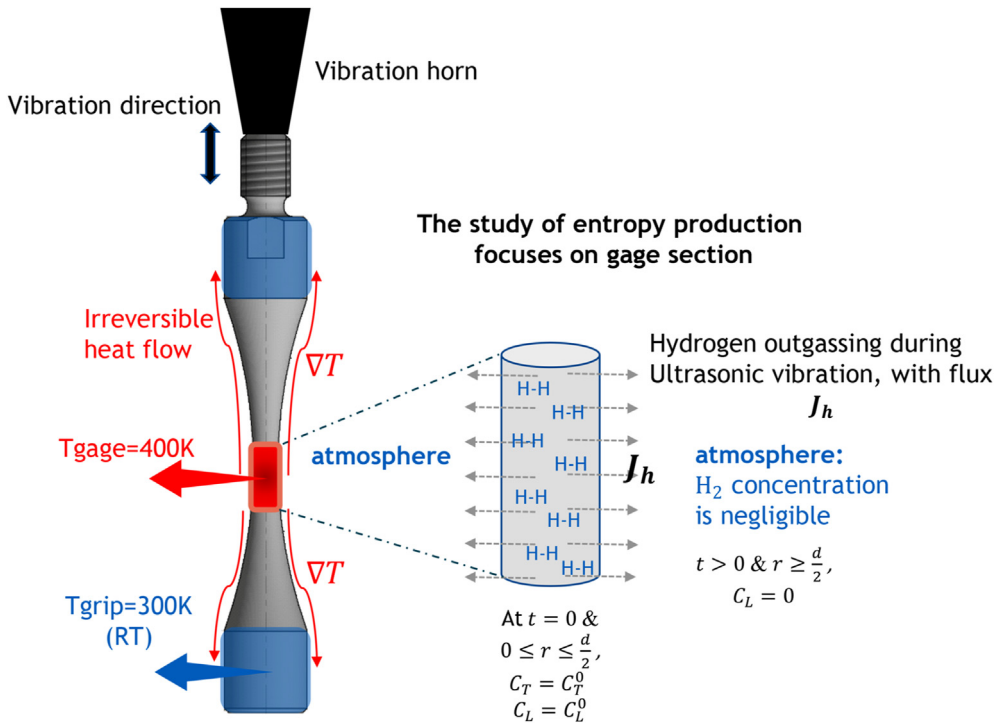

Fig. 8 – Schematic illustration of the hydrogen outgassing from the sample to the atmosphere during the ultrasonic vibration fatigue test.

Please cite this article as: Lee HW et al., Modeling fatigue life and hydrogen embrittlement of bcc steel with unified mechanics theory, International Journal of Hydrogen Energy, https://doi.org/10.1016/j.ijhydene.2023.02.110

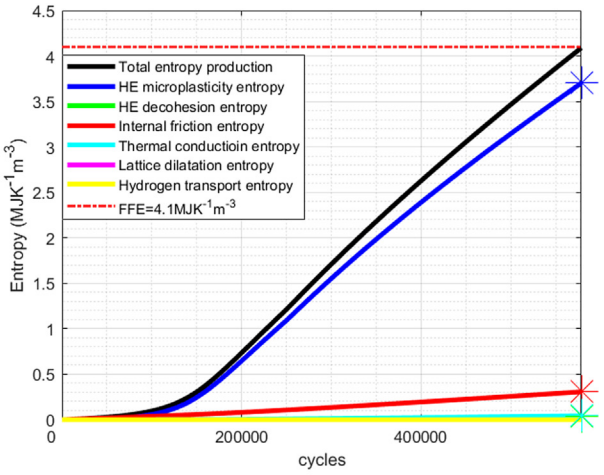

(a)

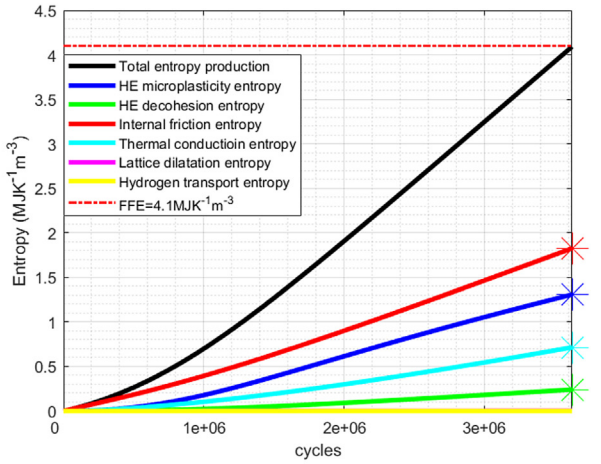

(b)

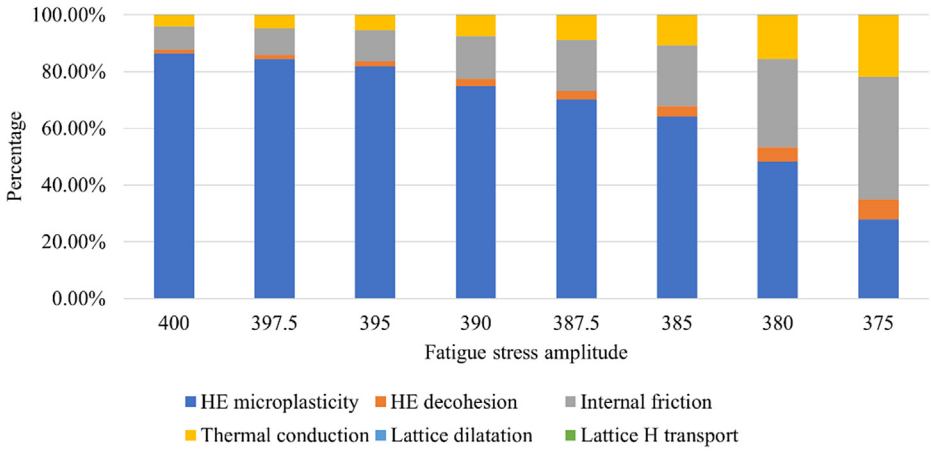

(c)

Fig. 9 – Comparison of entropy production due to different entropy generation sources during fatigue loading and hydrogen embrittlement. The number of cycles was increased until total entropy production reaches fatigue fracture entropy (FFE): (a) Stress amplitude is at 400 MPa, and the hydrogen-enhanced parameter $\tilde{\Psi} = 0.551$ is used considering $C_T = 0.5C_0$, (b) Stress amplitude is at 375 MPa, and the hydrogen-enhanced parameter $\tilde{\Psi} = 0.551$ is used considering $C_T = 0.5C_0$, (c) Entropy contribution percentage of each mechanism under different vibration stress amplitudes, considering $C_T = 0.5C_0$.

Please cite this article as: Lee HW et al., Modeling fatigue life and hydrogen embrittlement of bcc steel with unified mechanics theory, International Journal of Hydrogen Energy, https://doi.org/10.1016/j.ijhydene.2023.02.110

Table 3 – Comparison of the order of magnitude of entropy generation due to corrosion, mechanical loading, and hydrogen-enhanced mechanisms during ultrasonic fatigue loading.

Source[a]	Entropy generation mechanism	The magnitude of entropy generation
C	Corrosion activation overpotential	$\approx MJ \cdot K^{-1} \cdot m^{-3}$
M	Thermal conduction	$\approx MJ \cdot K^{-1} \cdot m^{-3}$
M	Internal friction	$\approx MJ \cdot K^{-1} \cdot m^{-3}$
M&H	Hydrogen-enhanced micro-plasticity (HEL(M)P)	$\approx MJ \cdot K^{-1} \cdot m^{-3}$
M&H	Hydrogen-enhanced decohesion (HEDE)	$\approx MJ \cdot K^{-1} \cdot m^{-3}$
H	Hydrogen transport	$\approx J \cdot K^{-1} \cdot m^{-3}$
H	Hydrogen dilatation	$\approx KJ \cdot K^{-1} \cdot m^{-3}$

[a] C: corrosion; M: mechanical loading; H: hydrogen-enhanced mechanism.

mechanisms at higher stress amplitude (e.g., 400 MPa), which can result in a ductile fracture when the fatigue life is reached. However, at lower stress amplitude (especially when stress amplitude is near the fatigue limit. e.g., 375 MPa), the contribution of internal friction greatly increases and becomes dominant. At the same time, the HELP and HEDE mechanisms of HE have a similar order of magnitude entropy contributions. We can expect to have a brittle fracture at 375 MPa stress amplitude. This simulation result matches well with the experimental evidence in the literature reviewed in the Introduction section and subsection Synergy of different hydrogen embrittlement mechanisms of this manuscript.

Fig. 9 shows a comparison of entropy generation for each micro mechanism of hydrogen embrittlement, including HEL(M)P, and HEDE. Entropy generation due to mechanical loading, internal friction, and thermal conduction must be considered in the thermodynamic fundamental equation. In comparison, the remaining entropy generation mechanisms, such as hydrogen transport and hydrogen-induced dilatation, are negligible and can be ignored. Because the corrosion for hydrogen pre-charging is not performed concurrently with the fatigue loading, the corrosion entropy production due to activation overpotential is not shown in Fig. 9. However, based on Fig. 6, it has the same order of magnitude as thermal conduction, which should also be considered in the thermodynamic fundamental equation if the ultrasonic vibration is conducted in a hydrogen-rich environment.

The effect of fatigue stress amplitude on fracture surface is explained and validated by identifying dominant entropy generation mechanisms at different stress levels. More sweeping C_T values must be tried in the parametric study to explore the effect of trapping hydrogen concentration on a material's fatigue behavior based on entropy production.

Thermodynamic state index (TSI) evolution and simulated fatigue S–N curves for the hydrogen pre-charged steel

The thermodynamic lifespan travels between 0 and near 1 along this axis. Based on the cumulative specific entropy production given by equation (50), the fatigue life of the hydrogen pre-charged structural steel can be estimated. However, it should be emphasized that before the fatigue test, the corrosion during hydrogen charging causes initial entropy production. Therefore, the TSI at the beginning of ultrasonic vibrations does not start from zero.

In this section, we make several assumptions about the material properties to be able to perform the parametric study. This section aims to show the effect of the increasing hydrogen concentration on fatigue life.

1. The steel samples were pre-charged with hydrogen through electrochemical corrosion in a $1MH_2SO_4$ solution. Assuming the corrosion takes 4 weeks, and the electrochemical parameters are constant throughout the process (Table 2, Electrochemical parameters).
2. The total hydrogen concentration is equivalent to the summation of concentration in trapping sites C_T (trapped hydrogen) and the concentration in lattice sites C_L (diffusible hydrogen), $C = C_T + C_L$.The diffusible hydrogen concentration C_L outgasses during the fatigue loading due to mechanical energy input and rising temperature, and the trapping concentration C_T changes due to plastic strain. They are related to each other by Oriani's theory (equation (38)). Here, a constant C_T is assumed for simplification. Because there is no loading during hydrogen pre-charging and fatigue load is in the elastic regime.

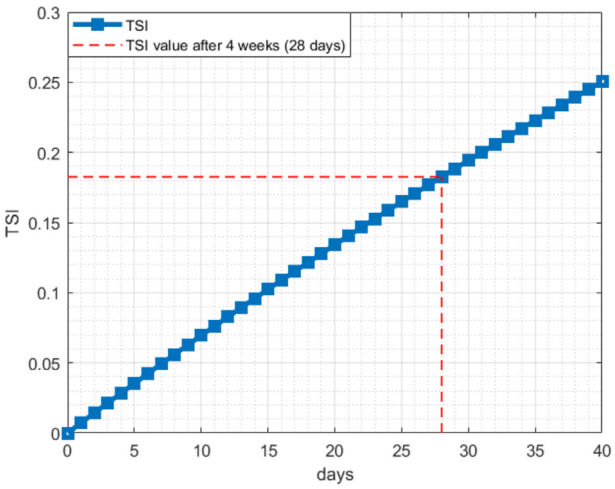

Fig. 10 – TSI evolution of the S355J2+N steel samples during the hydrogen charging process, based on the electrochemical constants given in Table 2.

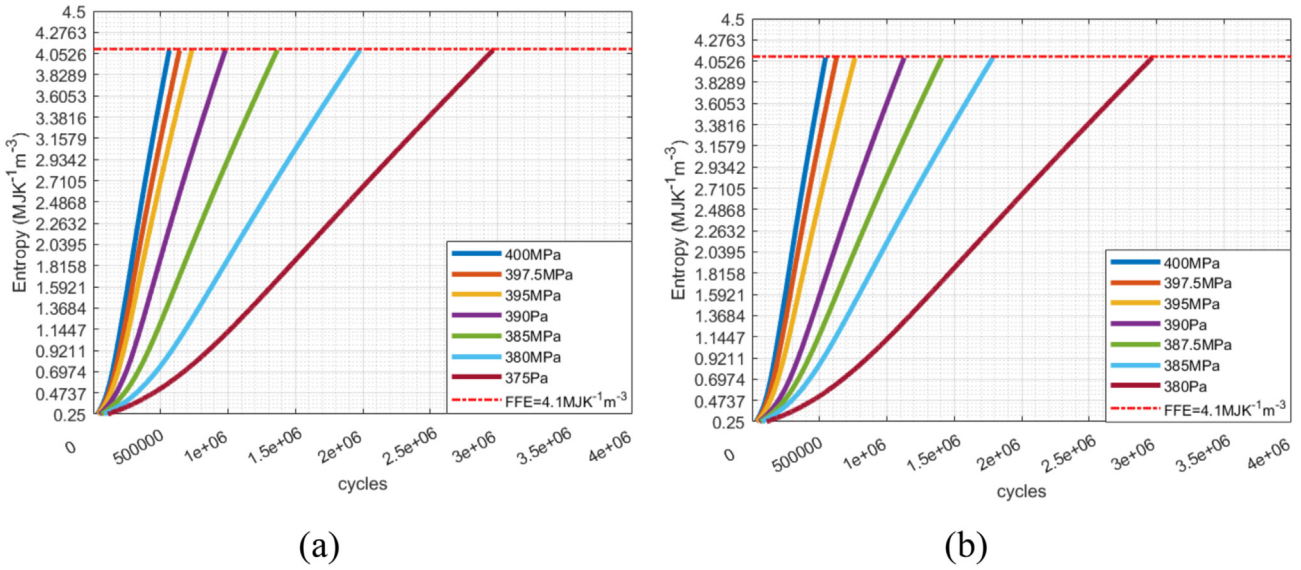

Fig. 11 – Cumulative entropy production of the hydrogen pre-charged S355J2+N steel samples subjected to ultrasonic vibration fatigue at various stress amplitudes, with a trapping hydrogen concentration of (a) $C_T = 0.25C_0$ and (b) $C_T = 0.5C_0$.

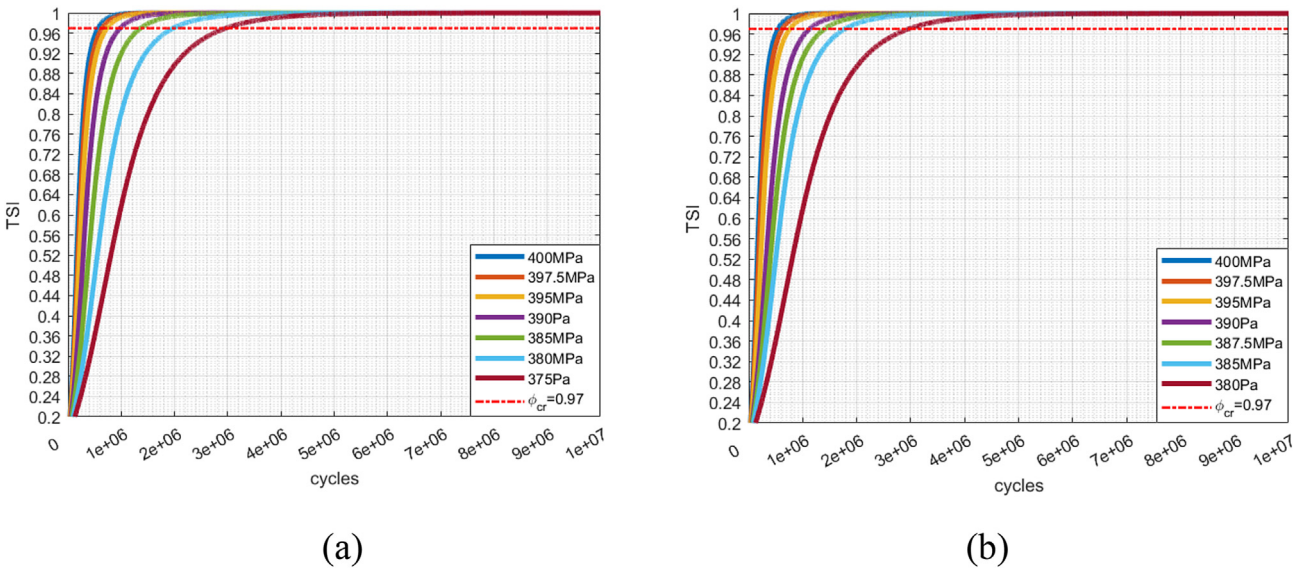

Fig. 12 – TSI evolution of the hydrogen pre-charged S355J2+N steel samples subjected to ultrasonic vibration fatigue at various stress amplitudes, with a trapping hydrogen concentration of (a) $C_T = 0.25C_0$ and (b) $C_T = 0.5C_0$.

3. It has been shown that hydrogen can induce enhanced plastic behavior or decohesion behavior depending on the concentration. Therefore, three sets of hydrogen concentration-dependent material constants in Table 2, Hydrogen enhanced microplastic strain rate function parameters for equations, were calculated based on equations (24–26) assuming $C_T = 0$, $C_T = 0.25C_0$, and $C_T = 0.5C_0$, respectively.

The reference microscopic yield stress parameter $\tilde{y}$ was chosen to be 354 MPa instead of 368 MPa as given in Table 2, Material parameters of steel sample. Because the corrosion causes degradation of the material; therefore, the fatigue limit is reduced. The fatigue limit, 354 MPa, is obtained from the experimental S–N curve of the sample corroded in NaCl solution [76]. We use this value for the parametric study.

Fig. 10 gives the TSI evolution during the hydrogen charging process, based on the entropy generation depicted in Fig. 6. It is observed that after 4-weeks of corrosion (in 1 M H_2SO_4) before fatigue testing, results in 0.18 coordinate on the TSI axis. For simplicity in the parametric study, we will use 0.2 TSI value as the starting value in Fig. 12. The duration of hydrogen charging is determined based on previous studies in the literature. Fig. 11 shows the entropy production of the

Please cite this article as: Lee HW et al., Modeling fatigue life and hydrogen embrittlement of bcc steel with unified mechanics theory, International Journal of Hydrogen Energy, https://doi.org/10.1016/j.ijhydene.2023.02.110

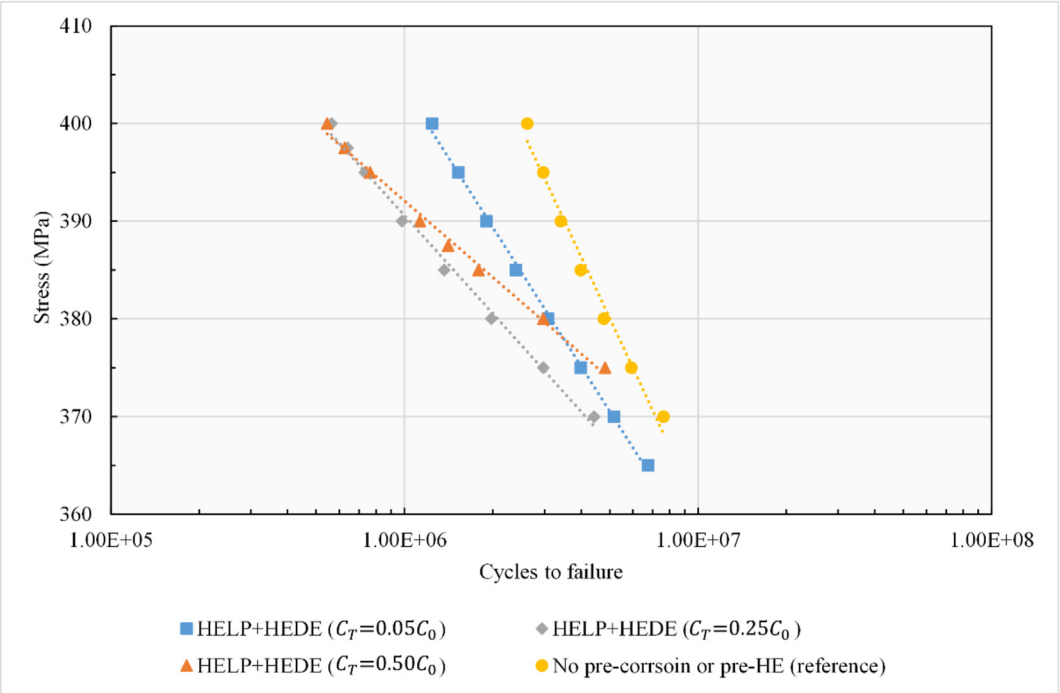

Fig. 13 – UMT-based simulated ultrasonic vibration fatigue S–N curves for the hydrogen pre-charged S355J2+N steel samples (HELP + HEDE model) at different hydrogen trapping concentration levels C_T compared to reference sample.

hydrogen pre-charged sample during ultrasonic vibration fatigue with a constant $C_T = 0.25C_0$ and $C_T = 0.5C_0$, respectively. Similarly, they start with the initial cumulative entropy value of 0.25 kJ/m^3 according to Fig. 6, instead of zero.

Fig. 12 shows the TSI evolution for both cases, respectively. It can be observed that the number of cycles to reach fatigue fracture entropy (FFE) or critical TSI is less in the case of $C_T = 0.5C_0$ (the fatigue life is reduced). Fig. 13 shows the simulated stress vs. number of cycles to failure (S–N) curve for the hydrogen pre-charged S355J2+N steel samples, at different trapped hydrogen concentrations.

In Fig. 11, the cumulative entropy production at failure (fatigue fracture entropy [71]) is a constant value regardless of stress amplitude, specimen dimension and geometry, and loading frequency. This constant value is called fatigue fracture entropy (FFE), which is well established in the literature [70–76,161]. In the simulation, the FFE is obtained upon the evolution of the TSI reaching the critical value. Based on equations (3) and (4), if a critical TSI $\Phi_{cr} = 0.97$ is chosen and the molar mass is given by $m_s = 55.7388$ g/mol, then the FFE can be easily calculated as follows,

$$\Delta s_{FFE} = -\ln(1-\Phi_{cr})\frac{R}{m_s} = 0.523\ \mathrm{J\cdot mol^{-1}\cdot g^{-1}} \tag{60}$$

If we multiply the result from equation (60) by the density of the material $\rho = 7.82$ g·cm^{-3}, the FFE is found to be 4.089 J·mol^{-1}·cm^{-3} or 4.089 MJ·mol^{-1}·m^{-3}, which is the result shown in Fig. 11 when fatigue life is reached. As a reference, the measured FFE for S355J2 + N steel (ASTM A656) is 4.1 MJ·mole^{-1}·m^{-3} [75]. In equation (60), the molar mass $m_s = 55.7388$ g/mol is used, which is obtained from equation (61):

$$m_s = (0.12\cdot m_C + 0.19\cdot m_{Si} + 1.29\cdot m_{Mn} + 0.004\cdot m_P + 0.015\cdot m_S + 0.2\cdot m_{Cu} + 98.181\cdot m_{Fe})/100 \tag{61}$$

where m_C, m_{Si}, m_{Mn}, m_P, m_S, m_{Cu}, and m_{Fe} are the molar mass of each main chemical component. They are given by $m_C = 12.011$, $m_{Si} = 28.0855$, $m_{Mn} = 54.9380$, $m_P = 30.9738$, $m_S = 32.065$, $m_{Cu} = 63.546$, and $m_{Fe} = 55.845$, all in units of g/mol.

In Fig. 12, there are seven branches each representing the TSI evolution for a sample under a specific linear elastic fatigue. The TSI evolution is an exponential equation shown in equation (3). The evolution of TSI is governed by the entropy production, Fig. 11. Once the TSI value reaches critical value TSI $\Phi_{cr} = 0.97$, the simulation stops; see equation (4). Then the number of cycles to reach $\Phi_{cr} = 0.97$ is the fatigue life of the sample under its corresponding linear elastic fatigue stress amplitude. Therefore, Fig. 12 shows the relation between the fatigue life and stress amplitude, which allows the establishment of a UMT-based stress-number of cycles to failure curve, as shown in Fig. 13.

From Fig. 13, it is clear that the fatigue life of hydrogen pre-charged steel will be reduced compared to the reference sample (no pre-corrosion or pre-HE). The fatigue life reduction from the reference sample to $C_T = 0.05C_0$ sample mainly results from the decrease of microscopic yield stress due to corrosion damage during hydrogen pre-charging. As for the comparison between three hydrogen-charged samples at different H trapping concentrations ($C_T = 0.05, 0.25,$ and $0.5\ C_0$), the reason for fatigue reduction is because of the increasing trapped hydrogen

Please cite this article as: Lee HW et al., Modeling fatigue life and hydrogen embrittlement of bcc steel with unified mechanics theory, International Journal of Hydrogen Energy, https://doi.org/10.1016/j.ijhydene.2023.02.110

concentration C_T induces greater hydrogen-enhanced microplastic strain (HEL(M)P), according to equations (22) and (24). However, meanwhile, the hardening modulus $\tilde{H}$ and yield stress $\tilde{y}$ are slightly increased due to higher C_T that cause the material to become more brittle and less ductile. Therefore, higher trapped hydrogen concentration does not lead to fatigue life reduction, particularly at fatigue stress amplitudes below 395 MPa, see S–N curves for higher $C_T = 0.5C_0$ vs $C_T = 0.25C_0$ shown in Fig. 13. It should also be emphasized that this result only applies to ultrasonic vibration fatigue, which operates at 20 KHz cyclic loadings within the material's linear elastic range. Because according to our model, the density of H trapping sites at dislocations $N_T^{(d)}$ remains constant (equation (40) and (41), see Table 1) at various fatigue stress amplitudes. In comparison, $N_T^{(d)}$ in a low cycle fatigue will be affected by the stress level due to the different amounts of plastic strain that elevate $N_T^{(d)}$ value during the fatigue process. However, the constant $N_T^{(d)}$ value, in very high cycle fatigue, lowers the contribution from the HEDE mechanism of HE, see Fig. 9 (c).

Conclusions

The thermodynamic fundamental equation of low-carbon ferrite-pearlite structural steel (S355J2+N) subjected to hydrogen embrittlement (HE) effects before ultrasonic vibration fatigue testing is derived.

The entropy generation mechanisms due to mechanical loading are mainly composed of temperature gradient-induced thermal conduction, fast-moving dislocation motion-induced internal friction, and stress concentration-induced micro-plasticity. Also, the entropy generation mechanisms due to electrochemical corrosion resulting from the activation overpotential are briefly introduced.

The entropy generation mechanisms due to hydrogen-enhanced mechanisms that include the sources from the synergistic action of HELP and HEDE mechanisms of hydrogen embrittlement (HELP + HEDE model) are explored and modified for the case of ultrasonic vibration fatigue that operates at a stress amplitude well below the yield stress. Also, a novel two-stage model for synergistic action of multiple active HE mechanisms (HELP + HEDE model) and microplasticity, including the effects of both hydrogen-enhanced microplasticity (HEL(M)P) and hydrogen-enhanced decohesion, during very high cycle fatigue, was proposed and applied. Using the model, stress versus the number of cycles to failure S–N curves are generated for parametric study. The fatigue life of hydrogen pre-charged steel will be reduced compared to the reference sample due to the synergistic action of HELP and HEDE mechanisms of HE depending on the hydrogen trapping concentration levels C_T and applied stress amplitudes.

It is observed that at higher stress amplitudes, microplasticity entropy production is the most dominant entropy generation mechanism. However, at lower stress amplitude the contribution of microplasticity and hydrogen-enhanced microplasticity (HEL(M)P) is reduced. Instead, the contribution from internal friction and the HEDE mechanism of hydrogen embrittlement increases. These results match well with the SEM studies of the fracture surfaces published in the literature. At a median to high-stress level during ultrasonic vibration fatigue, such as 400 MPa, a micro void coalescence-induced ductile fracture is expected, which can be attributed to microplasticity. Whereas at low-stress levels, such as 375 MPa, cracks initiate at surface defects, causing the fracture to be brittle. The role of hydrogen here is to increase the microplastic entropy production at the median to high-stress level by enhancing the microplastic strain, causing a faster ductile failure (HEL(M)P), or increasing the HEDE entropy at a low-stress level, causing a brittle failure.

However, the effect of critical hydrogen concentration on fracture behavior at low or high-stress amplitudes and the exact degree of activity of both HELP and HEDE mechanisms of hydrogen embrittlement, cannot be interpreted directly from the current model. Because, unlike low cycle fatigue, ultrasonic vibration fatigue is in an elastic regime and does not generate macroscopic plastic strain that increases the trapping of hydrogen during fatigue loading, which leads to the increase of decohesion entropy (HEDE) and brittle failure at high hydrogen concentrations.

This UMT modeling study provides for the first-time results for entropy production due to the synergistic action of hydrogen embrittlement mechanisms (HELP + HEDE model) in hydrogen pre-charged steel. It mainly focuses on theoretical modeling and parametric study. The discussion of the experimental data and comparison with the UMT model presented in this paper is envisaged in our next publication. Finally, we should emphasize that this work is for the general discussion of the ultrasonic vibration fatigue behavior of low carbon bcc steel S355J2+N, equivalent to ASTM A656 when it is pre-charged with hydrogen (hydrogen embrittled).

Declaration of competing interest

The authors declare that they have no known competing financial interests or personal relationships that could have appeared to influence the work reported in this paper.

REFERENCES

[1] Basaran C. Introduction to unified mechanics theory with applications. 2nded. Germany: Springer Nature: Berlin/Heidelberg; 2023. 2023; ISBN 978-3-031-18620-2.
[2] Wasim M, Djukic MB. External corrosion of oil and gas pipelines: a review of failure mechanisms and predictive preventions. J Nat Gas Sci Eng 2022;100:104467. https://doi.org/10.1016/j.jngse.2022.104467.
[3] Trško L, Nový F, Bokůvka O, Jambor M. Ultrasonic fatigue testing in the tension-compression mode. JoVE 2018;133:e57007. https://doi.org/10.3791/57007.
[4] Li H, Niu R, Li W, Lu H, Cairney J, Chen Y-S. Hydrogen in pipeline steels: recent advances in characterization and embrittlement mitigation. J Nat Gas Sci Eng 2022;105:104709. https://doi.org/10.1016/j.jngse.2022.104709.
[5] Laureys A, Depraetere R, Cauwels M, Depover T, Hertelé S, Verbeken K. Use of existing steel pipeline infrastructure for gaseous hydrogen storage and transport: a review of factors affecting hydrogen-induced degradation. J Nat Gas Sci Eng 2022;101:104534. https://doi.org/10.1016/j.jngse.2022.104534.

Please cite this article as: Lee HW et al., Modeling fatigue life and hydrogen embrittlement of bcc steel with unified mechanics theory, International Journal of Hydrogen Energy, https://doi.org/10.1016/j.ijhydene.2023.02.110

[6] Bouledroua O, Hafsi Z, Djukic MB, Elaoud S. The synergistic effects of hydrogen embrittlement and transient gas flow conditions on integrity assessment of a precracked steel pipeline. Int J Hydrogen Energy 2020;45(35):18010–20. https://doi.org/10.1016/j.ijhydene.2020.04.262.
[7] Michler T, Wackermann K, Schweizer F. Review and assessment of the effect of hydrogen gas pressure on the embrittlement of steels in gaseous hydrogen environment. Metals 2021;11(4):637. https://doi.org/10.3390/met11040637.
[8] Marchi C, Somerday BP, Robinson SL. Permeability, solubility, and diffusivity of hydrogen isotopes in stainless steels at high gas pressures. Int J Hydrogen Energy 2007;32(1):100–16. https://doi.org/10.1016/j.ijhydene.2006.05.008.
[9] Djukic MB, Bakic GM, Sijacki Zeravcic V, Sedmak A, Rajicic B. The synergistic action and interplay of hydrogen embrittlement mechanisms in steels and iron: localized plasticity and decohesion. Eng Fract Mech 2019;216:106528. https://doi.org/10.1016/j.engfracmech.2019.106528.
[10] Popov BN, Lee J-W, Djukic MB. Hydrogen permeation and hydrogen-induced cracking. Handb Environ Degrad Mater 2018:133–62. https://doi.org/10.1016/b978-0-323-52472-8.00007-1.
[11] Djukic MB, Sijacki Zeravcic V, Bakic GM, Sedmak A, Rajicic B. Hydrogen damage of Steels: a case study and hydrogen embrittlement model. Eng Fail Anal 2015;58:485–98. https://doi.org/10.1016/j.engfailanal.2015.05.017.
[12] Murakami Y, Kanezaki T, Mine Y, Matsuoka S. Hydrogen embrittlement mechanism in fatigue of austenitic stainless steels. Metall Mater Trans 2008;39(6). https://doi.org/10.1007/s11661-008-9506-5.
[13] Kishi A, Takano N. Effect of hydrogen cathodic charging on fatigue fracture of type 310s stainless steel. J Phys Conf 2010;240:012050. https://doi.org/10.1088/1742-6596/240/1/012050.
[14] Brück S, Schippl V, Schwarz M, Christ H-J, Fritzen C-P, Weihe S. Hydrogen embrittlement mechanism in fatigue behavior of austenitic and martensitic stainless steels. Metals 2018;8(5):339. https://doi.org/10.3390/met8050339.
[15] Nahm S-H, Shim H-B, Baek U-B, Suh C-M. Very high cycle fatigue behaviors and surface crack growth mechanism of hydrogen-embrittled AISI 304 Stainless Steels. Mater Sci Appl 2018;9(4):393–411. https://doi.org/10.4236/msa.2018.94027.
[16] Bal B, Çetin B, Bayram FC, Billur E. Effect of hydrogen on fracture locus of Fe–16Mn–0.6C–2.15Al TWIP steel. Int J Hydrogen Energy 2020;45(58):34227–40. https://doi.org/10.1016/j.ijhydene.2020.09.083.
[17] Baltacioglu MF, Cetin B, Bal B. The effect of strain rate on the hydrogen embrittlement susceptibility of aluminum 7075. J Eng Mater Technol 2022;145(2). https://doi.org/10.1115/1.4056158.
[18] Bal B, Okdem B, Bayram FC, Aydin M. A detailed investigation of the effect of hydrogen on the mechanical response and microstructure of Al 7075 alloy under medium strain rate impact loading. Int J Hydrogen Energy 2020;45(46):25509–22. https://doi.org/10.1016/j.ijhydene.2020.06.241.
[19] Fassina P, Brunella F, Lazzari L, Re G, Vergani L, Sciuccati A. Fatigue behavior of pipeline steel under hydrogen environment and low temperature. Procedia Eng 2011;10:3345–52. https://doi.org/10.1016/j.proeng.2011.04.552.
[20] Lee SG, Kim IS. Effect of pre-charged hydrogen on fatigue crack growth of low alloy steel at 288°C. Mater Sci Eng, A 2006;420(1–2):279–85. https://doi.org/10.1016/j.msea.2006.01.080.
[21] Tsuchida Y, Watanabe T, Suzuki G, Yano H. Cyclic deformation behavior and low cycle fatigue life of normalized medium carbon steel with hydrogen charging. Procedia Eng 2011;10:1176–83. https://doi.org/10.1016/j.proeng.2011.04.196.
[22] Rajabipour A, Melchers RE. Application of Paris law for estimation of hydrogen-assisted fatigue crack growth. Int J Fatig 2015;80:357–63. https://doi.org/10.1016/j.ijfatigue.2015.06.027.
[23] An T, Peng H, Bai P, Zheng S, Wen X, Zhang L. Influence of hydrogen pressure on fatigue properties of X80 Pipeline Steel. Int J Hydrogen Energy 2017;42(23):15669–78. https://doi.org/10.1016/j.ijhydene.2017.05.047.
[24] Yamabe J, Yoshikawa M, Matsunaga H, Matsuoka S. Hydrogen trapping and fatigue crack growth property of low-carbon steel in the hydrogen-gas environment. Int J Fatig 2017;102:202–13. https://doi.org/10.1016/j.ijfatigue.2017.04.010.
[25] Dmytrakh IM, Leshchak RL, Syrotyuk AM, Barna RA. Effect of hydrogen concentration on fatigue crack growth behaviour in Pipeline Steel. Int J Hydrogen Energy 2017;42(9):6401–8. https://doi.org/10.1016/j.ijhydene.2016.11.193.
[26] Djukic MB, Bakic GM, Sijacki Zeravcic V, Sedmak A, Rajicic B. Hydrogen embrittlement of industrial components: prediction, prevention, and Models. Corrosion 2016;72(7):943–61. https://doi.org/10.5006/1958.
[27] Zhao T, Liu Z, Xu X, Li Y, Du C, Liu X. Interaction between hydrogen and cyclic stress and its role in fatigue damage mechanism. Corrosion Sci 2019;157:146–56. https://doi.org/10.1016/j.corsci.2019.05.028.
[28] Balitskii A, Vytvytskyii V, Ivaskevich L, Eliasz J. The high- and low-cycle fatigue behavior of Ni-contain steels and Ni-alloys in high pressure hydrogen. Int J Fatig 2012;39:32–7. https://doi.org/10.1016/j.ijfatigue.2011.05.017.
[29] Nygren KE, Nagao A, Wang S, Sofronis P, Robertson IM. Influence of internal hydrogen content on the evolved microstructure beneath fatigue striations in 316L austenitic stainless steel. Acta Mater 2021;213:116957. https://doi.org/10.1016/j.actamat.2021.116957.
[30] Oliveira DM, San Marchi CW, Medlin DL, Gibeling JC. The influence of hydrogen on the low cycle fatigue behavior of strain-hardened 316L stainless steel. Mater Sci Eng, A 2022;849:143477. https://doi.org/10.1016/j.msea.2022.143477.
[31] Vergani L, Colombo C, Gobbi G, Bolzoni FM, Fumagalli G. Hydrogen effect on fatigue behavior of a quenched & tempered steel. Procedia Eng 2014;74:468–71. https://doi.org/10.1016/j.proeng.2014.06.299.
[32] Colombo C, Fumagalli G, Bolzoni F, Gobbi G, Vergani L. Fatigue behavior of hydrogen pre-charged low alloy Cr–Mo steel. Int J Fatig 2016;83:2–9. https://doi.org/10.1016/j.ijfatigue.2015.06.002.
[33] Pradhan A, Vishwakarma M, Dwivedi SK. A review: the impact of hydrogen embrittlement on the fatigue strength of high strength steel. Mater Today Proc 2020;26:3015–9. https://doi.org/10.1016/j.matpr.2020.02.627.
[34] Li YD, Yang ZG, Liu YB, Li SX, Li GY, Hui WJ, Weng YQ. The influence of hydrogen on very high cycle fatigue properties of high strength spring steel. Mater Sci Eng, A 2008;489(1–2):373–9. https://doi.org/10.1016/j.msea.2008.01.089.
[35] Bruchhausen M, Fischer B, Ruiz A, González S, Hähner P, Soller S. Impact of hydrogen on the high cycle fatigue behaviour of Inconel 718 in asymmetric push–pull mode at room temperature. Int J Fatig 2015;70:137–45. https://doi.org/10.1016/j.ijfatigue.2014.09.005.
[36] Kirchheim R. Revisiting hydrogen embrittlement models and hydrogen-induced homogeneous nucleation of

Please cite this article as: Lee HW et al., Modeling fatigue life and hydrogen embrittlement of bcc steel with unified mechanics theory, International Journal of Hydrogen Energy, https://doi.org/10.1016/j.ijhydene.2023.02.110

dislocations. Scripta Mater 2010;62(2):67–70. https://doi.org/10.1016/j.scriptamat.2009.09.037.
[37] Deutges M, Barth HP, Chen Y, Borchers C, Kirchheim R. Hydrogen diffusivities as a measure of relative dislocation densities in palladium and increase of the density by plastic deformation in the presence of dissolved hydrogen. Acta Mater 2015;82:266–74. https://doi.org/10.1016/j.actamat.2014.09.013.
[38] Kirchheim R. Lattice discontinuities affecting the generation and annihilation of diffusible hydrogen and vice versa. Phil Trans Math Phys Eng Sci 2017;375(2098):20160403. https://doi.org/10.1098/rsta.2016.0403. 2098.
[39] Wasim M, Djukic MB, Ngo TD. Influence of hydrogen-enhanced plasticity and decohesion mechanisms of hydrogen embrittlement on the fracture resistance of steel. Eng Fail Anal 2021;123:105312. https://doi.org/10.1016/j.engfailanal.2021.105312.
[40] Dadfarnia M, Nagao A, Wang S, Martin ML, Somerday BP, Sofronis P. Recent advances on hydrogen embrittlement of structural materials. Int J Fract 2015;196(1–2):223–43. https://doi.org/10.1007/s10704-015-0068-4.
[41] Koyama M, Akiyama E, Tsuzaki K, Raabe D. Hydrogen-assisted failure in a twinning-induced plasticity steel studied under in situ hydrogen charging by electron channeling contrast imaging. Acta Mater 2013;61(12):4607–18. https://doi.org/10.1016/j.actamat.2013.04.030.
[42] Wang M, Akiyama E, Tsuzaki K. Effect of hydrogen and stress concentration on the notch tensile strength of AISI 4135 steel. Mater Sci Eng, A 2005;398(1–2):37–46. https://doi.org/10.1016/j.msea.2005.03.008.
[43] Wang M, Akiyama E, Tsuzaki K. Effect of hydrogen on the fracture behavior of high strength steel during slow strain rate test. Corrosion Sci 2007;49(11):4081–97. https://doi.org/10.1016/j.corsci.2007.03.038.
[44] Koyama M, Akiyama E, Sawaguchi T, Raabe D, Tsuzaki K. Hydrogen-induced cracking at grain and twin boundaries in an Fe–Mn–C austenitic steel. Scripta Mater 2012;66(7):459–62. https://doi.org/10.1016/j.scriptamat.2011.12.015.
[45] Kwon YJ, Seo HJ, Kim JN, Lee CS. Effect of grain boundary engineering on hydrogen embrittlement in Fe-Mn-C TWIP steel at various strain rates. Corrosion Sci 2018;142:213–21. https://doi.org/10.1016/j.corsci.2018.07.028.
[46] Wasim M, Djukic MB. Corrosion induced failure of the ductile iron pipes at micro- and nano-levels. Eng Fail Anal 2021;121:105169. https://doi.org/10.1016/j.engfailanal.2020.105169.
[47] Maier HJ, Popp W, Kaesche H. A method to evaluate the critical hydrogen concentration for hydrogen-induced crack propagation. Acta Metall 1987;35(4):875–80. https://doi.org/10.1016/0001-6160(87)90164-7.
[48] Dmytrakh IM, Leshchak RL, Syrotyuk AM. Effect of hydrogen concentration on strain behaviour of pipeline steel. Int J Hydrogen Energy 2015;40(10):4011–8. https://doi.org/10.1016/j.ijhydene.2015.01.094.
[49] Lunarska E. Correlation between critical hydrogen concentration and hydrogen damage of pipeline steel. Int J Hydrogen Energy 1997;22(2–3):279–84. https://doi.org/10.1016/s0360-3199(96)00178-4.
[50] Hanneken J. Hydrogen in metals and other materials: a comprehensive reference to books, bibliographies, workshops and conferences. Int J Hydrogen Energy 1999;24(10):1005–26. https://doi.org/10.1016/s0360-3199(98)00137-2.
[51] Capelle J, Gilgert J, Dmytrakh I, Pluvinage G. The effect of hydrogen concentration on fracture of pipeline steels in presence of a notch. Eng Fract Mech 2011;78(2):364–73. https://doi.org/10.1016/j.engfracmech.2010.10.007.
[52] Lovicu G, Bottazzi M, D'Aiuto F, De Sanctis M, Dimatteo A, Santus C, Valentini R. Hydrogen embrittlement of automotive advanced high-strength steels. Metall Mater Trans 2012;43(11):4075–87. https://doi.org/10.1007/s11661-012-1280-8.
[53] Wang M, Akiyama E, Tsuzaki K. Determination of the critical hydrogen concentration for delayed fracture of high strength steel by constant load test and numerical calculation. Corrosion Sci 2006;48(8):2189–202. https://doi.org/10.1016/j.corsci.2005.07.010.
[54] Murakami Y, Kanezaki T, Mine Y. Hydrogen effect against hydrogen embrittlement. Metall Mater Trans 2010;41(10):2548–62. https://doi.org/10.1007/s11661-010-0275-6.
[55] Matsui H, Kimura H, Moriya S. The effect of hydrogen on the mechanical properties of high purity iron I. Softening and hardening of high purity iron by hydrogen charging during tensile deformation. Mater Sci Eng 1979;40(2):207–16. https://doi.org/10.1016/0025-5416(79)90191-5.
[56] Zhao Y, Seok M-Y, Choi I-C, Lee Y-H, Park S-J, Ramamurty U, Suh J-Y, Jang J. The role of hydrogen in hardening/softening steel: influence of the charging process. Scripta Mater 2015;107:46–9. https://doi.org/10.1016/j.scriptamat.2015.05.017.
[57] Wen M, Fukuyama S, Yokogawa K. Atomistic simulations of effect of hydrogen on kink-pair energetics of screw dislocations in bcc iron. Acta Mater 2003;51(6):1767–73. https://doi.org/10.1016/s1359-6454(02)00575-x.
[58] Wang S, Hashimoto N, Wang Y, Ohnuki S. Activation volume and density of mobile dislocations in hydrogen-charged iron. Acta Mater 2013;61(13):4734–42. https://doi.org/10.1016/j.actamat.2013.05.007.
[59] Ferreira PJ, Robertson IM, Birnbaum HK. Hydrogen effects on the interaction between dislocations. Acta Mater 1998;46(5):1749–57. https://doi.org/10.1016/s1359-6454(97)00349-2.
[60] Abraham DP, Altstetter CJ. Hydrogen-enhanced localization of plasticity in an austenitic stainless steel. Metall Mater Trans 1995;26(11):2859–71. https://doi.org/10.1007/bf02669644.
[61] Tabata T, Birnbaum HK. Direct observations of hydrogen enhanced crack propagation in iron. Scripta Metall 1984;18(3):231–6. https://doi.org/10.1016/0036-9748(84)90513-1.
[62] Katzarov IH, Pashov DL, Paxton AT. Hydrogen embrittlement I. Analysis of hydrogen-enhanced localized plasticity: effect of hydrogen on the velocity of screw dislocations inα-Fe. Phys Rev Mater 2017;1(3). https://doi.org/10.1103/physrevmaterials.1.033602.
[63] Taketomi S, Matsumoto R, Hagihara S. Molecular statics simulation of the effect of hydrogen concentration on {112}<111> edge dislocation mobility in alpha iron. ISIJ Int 2017;57(11):2058–64. https://doi.org/10.2355/isijinternational.isijint-2017-172.
[64] Djukic MB, Bakic GM, Sijacki Zeravcic V, Rajicic B, Sedmak A, Mitrovic R, Miskovic Z. A structural integrity model for hydrogen embrittlement of low carbon steel and the combined effect of help and hede mechanisms on macromechanical properties. ICF 2017 – 14th Int Conf Fract 2017;1:765–6.
[65] Wang J-S. The thermodynamics aspects of hydrogen induced embrittlement. Eng Fract Mech 2001;68(6):647–69. https://doi.org/10.1016/s0013-7944(00)00120-x.
[66] Lee HW, Basaran C. A review of damage, void evolution, and fatigue life prediction models. Metals 2021;11(4):609. https://doi.org/10.3390/met11040609.

Please cite this article as: Lee HW et al., Modeling fatigue life and hydrogen embrittlement of bcc steel with unified mechanics theory, International Journal of Hydrogen Energy, https://doi.org/10.1016/j.ijhydene.2023.02.110

[67] Boltzmann L. *Über die Beziehungzwischen dem zweitenHauptsatze des mechanischenWärmetheorie und der Wahrscheinlichkeitsrechnung, respective den Sätzenüber das Wärmegleichgewicht. [On the relation between the second law of the mechanical theory of heat and the probability calculus with respect to theorems of thermal equilibrium].* Wiener Berichte II 1877;76:373–435.
[68] Planck M. In: Vorlesungen über die theorie der wärmestrahlung. Leipzig: Barth; 1906. p. 163.
[69] Naderi M, Amiri M, Khonsari M. On the thermodynamic entropy of fatigue fracture. Proc Math Phys Eng Sci 2009;466(2114):423–38. https://doi.org/10.1098/rspa.2009.0348.
[70] Bin Jamal M,N, Kumar A, Lakshmana Rao C, Basaran C. Low cycle fatigue life prediction using unified mechanics theory in Ti-6Al-4V alloys. Entropy 2019;22(1):24. https://doi.org/10.3390/e22010024.
[71] Bin Jamal M,N, Rao CL, Basaran C. A unified mechanics theory-based model for temperature and strain rate dependent proportionality limit stress of mild steel. Mech Mater 2021;155:103762. https://doi.org/10.1016/j.mechmat.2021.103762.
[72] Bin Jamal M,N, Lee H, Lakshmana Rao C, Basaran C. Dynamic equilibrium equations in unified mechanics theory. Appl Mechan 2021;2(1):63–80. https://doi.org/10.3390/applmech2010005.
[73] Bin Jamal M,N, Chebolu LR, Basaran C. Unified Mechanics theory based flow stress model for the rate-dependent behavior of BCC Metals. Mater Today Commun 2022;31:103707. https://doi.org/10.1016/j.mtcomm.2022.103707.
[74] Lee HW, Basaran C. Predicting high cycle fatigue life with unified mechanics theory. Mech Mater 2022;164:104116. https://doi.org/10.1016/j.mechmat.2021.104116.
[75] Lee HW, Basaran C, Egner H, Lipski A, Piotrowski M, &Mroziński S, et al. Modeling ultrasonic vibration fatigue with unified mechanics theory. Int J Solid Struct 2021;236(237):111313. https://doi.org/10.1016/j.ijsolstr.2021.111313.
[76] Lee HW, Basaran C, Fakhri H, Ranade R, Egner H, Lipski A, Piotrowski M, &Mroziński S. Modeling fatigue of pre-corroded body-centered cubic metals with unified mechanics theory. Mater Des 2022;224:111383. https://doi.org/10.1016/j.matdes.2022.111383.
[77] Álvarez G, Zafra A, Belzunce FJ, Rodríguez C. Hydrogen embrittlement testing procedure for the analysis of structural steels with small punch tests using notched specimens. Eng Fract Mech 2021;253:107906. https://doi.org/10.1016/j.engfracmech.2021.107906.
[78] Wasim M, Djukic MB. Hydrogen embrittlement of low carbon structural steel at macro-, micro- and nano-levels. Int J Hydrogen Energy 2020;45(3):2145–56. https://doi.org/10.1016/j.ijhydene.2019.11.070.
[79] Popov B. Electrochemical kinetics of corrosion. CorroJ Assoc Arab Univer Basic Appl Scision Eng 2015:93–142. https://doi.org/10.1016/b978-0-444-62722-3.00003-3.
[80] Tait WS. An introduction to electrochemical corrosion testing for practicing engineers and scientists. PairODocs Publ; 1994.
[81] Gutman EM. Mechanochemistry of materials. Cambridge International Science Publishing; 1998.
[82] Imanian A, Modarres M. A thermodynamic entropy approach to reliability assessment with applications to corrosion fatigue. Entropy 2015;17(12):6995–7020. https://doi.org/10.3390/e17106995.
[83] Onsager L. Reciprocal relations in irreversible processes. I. Physical Review 1931;37(4):405–26. https://doi.org/10.1103/physrev.37.405.
[84] Kutz M. Handbook of environmental degradation of materials. William Andrew; 2018.
[85] Lim ChangHoon, MZB. Lecture 13: Butler-Volmer equation, electrochemical energy systems. MIT OpenCourseWare; 2014.
[86] Page CL. 5 - corrosion and protection of reinforcing steel in concrete. In: Durability of concrete and cement composites. Woodhead Publishing Series in Civil and Structural Engineering; 2007. p. 136–86. https://doi.org/10.1533/9781845693398.136.
[87] Fekry AM, Ameer MA. Electrochemical investigation on the corrosion and hydrogen evolution rate of mild steel in sulphuric acid solution. Int J Hydrogen Energy 2011;36(17):11207–15. https://doi.org/10.1016/j.ijhydene.2011.05.149.
[88] Ferhat M, Benchettara A, Amara SE, Najjar D. Corrosion behaviour of Fe-C alloys in a sulfuric medium. J Mater Environ Sci 2014;5(4):1059–68. ISSN: 2028-2508.
[89] Zheng X, Zhang S, Gong M, Li W. Experimental and theoretical study on the corrosion inhibition of mild steel by 1-octyl-3-methylimidazolium l-prolinate in sulfuric acid solution. Ind Eng Chem Res 2014;53(42):16349–58. https://doi.org/10.1021/ie502578q.
[90] Al-Amiery A, Kadhum A, Kadihum A, Mohamad A, How C, Junaedi S. Inhibition of mild steel corrosion in sulfuric acid solution by New Schiff Base. Materials 2014;7(2):787–804. https://doi.org/10.3390/ma7020787.
[91] Bammou L, Belkhaouda M, Salghi R, Benali O, Zarrouk A, Zarrok H, Hammouti B. Corrosion inhibition of steel in sulfuric acidic solution by the *chenopodium ambrosioides* extracts. Journal of the Association of Arab Universities for Basic and Applied Sciences 2014;16(1):83–90. https://doi.org/10.1016/j.jaubas.2013.11.001.
[92] S Al-Gorair A. Expired paracetamol as corrosion inhibitor for low carbon steel in sulfuric acid. electrochemical, kinetics and thermodynamics investigation. Int J Electrochem Sci 2021;16(7):1–16. https://doi.org/10.20964/2021.07.73. 210771.
[93] Akiyama E, Li S. Electrochemical hydrogen permeation tests under galvanostatic hydrogen charging conditions conventionally used for hydrogen embrittlement study. Corrosion Rev 2016;34(1–2):103–12. https://doi.org/10.1515/corrrev-2015-0049.
[94] Fuji H, Fujishiro T, Hara T. Effect of ammonium thiocyanate on hydrogen entry behavior of low alloy steel under galvanostatic cathode charging. ISIJ Int 2021;61(4):1151–8. https://doi.org/10.2355/isijinternational.isijint-2020-455.
[95] Ichiba M, Sakai J, Doshida T, Takai K. Corrosion reaction and hydrogen absorption of steel for prestressed concrete in a 20mass% ammonium thiocyanate solution. Scripta Mater 2015;102:59–62. https://doi.org/10.1016/j.scriptamat.2015.02.013.
[96] Ichimiya R, Nonaka K, Hiroike K, Takahashi A, Yamamoto N, Toyohiro T. Hydrogen Embrittlement Test on Dual Phase Steel using Aqueous Solution of Ammonium Thiocyanate. *International Conference on Science, Technology and Education* 2020;2020:11–5.
[97] Huang M, Rivera-Díaz-Del-Castillo PEJ, Bouaziz O, &Van Der Zwaag S. Irreversible thermodynamics modelling of plastic deformation of metals. Mater Sci Technol 2008;24(4):495–500. https://doi.org/10.1179/174328408X294125.
[98] De Hosson ThM, Roos A, E. D., Me J. Temperature rise due to fast-moving dislocations. Philos Mag A 2001;81(5):1099–120. https://doi.org/10.1080/01418610110033975.
[99] Fan H, Wang Q, El-Awady J, Raabe D, Zaiser M. Strain rate dependency of dislocation plasticity. Nat Commun 2021;12(1). https://doi.org/10.1038/s41467-021-21939-1.

Please cite this article as: Lee HW et al., Modeling fatigue life and hydrogen embrittlement of bcc steel with unified mechanics theory, International Journal of Hydrogen Energy, https://doi.org/10.1016/j.ijhydene.2023.02.110

[100] Galligan J, McKrell T, Robson M. Dislocation drag processes. Mater Sci Eng, A 2000;287(2):259–64. https://doi.org/10.1016/s0921-5093(00)00783-8.
[101] Chen X, Xiong L, McDowell DL, Chen Y. Effects of phonons on mobility of dislocations and dislocation arrays. Scripta Mater 2017;137:22–6. https://doi.org/10.1016/j.scriptamat.2017.04.033.
[102] Dwivedi SK, Vishwakarma M. Hydrogen embrittlement in different materials: a Review. Int J Hydrogen Energy 2018;43(46):21603–16. https://doi.org/10.1016/j.ijhydene.2018.09.201.
[103] Barrera O, Bombac D, Chen Y, Daff TD, Galindo-Nava E, Gong P, Haley D, Horton R, Katzarov I, Kermode JR, Liverani C, Stopher M, Sweeney F. Understanding and mitigating hydrogen embrittlement of Steels: a review of experimental, modelling and design progress from Atomistic to continuum. J Mater Sci 2018;53(9):6251–90. https://doi.org/10.1007/s10853-017-1978-5.
[104] Djukic MB, Zeravcic VS, Bakic G, Sedmak A, Rajicic B. Hydrogen embrittlement of low carbon structural steel. Proc Mater Sci 2014;3:1167–72. https://doi.org/10.1016/j.mspro.2014.06.190.
[105] Li X, Ma X, Zhang J, Akiyama E, Wang Y, Song X. Review of hydrogen embrittlement in metals: hydrogen diffusion, hydrogen characterization, hydrogen embrittlement mechanism and prevention. Acta Metall Sin 2020;33(6):759–73. https://doi.org/10.1007/s40195-020-01039-7.
[106] Robertson IM, Sofronis P, Nagao A, Martin ML, Wang S, Gross DW, Nygren KE. Hydrogen embrittlement understood. Metall Mater Trans B 2015;46(3):1085–103. https://doi.org/10.1007/s11663-015-0325-y.
[107] Zapffe CA, Sims CE. Papers - hydrogen embrittlement, internal stress and defects in steel. 1941. T.P. 1307, with discussion.
[108] Staehle RW, Forty AJ. Fundamental aspects of stress corrosion cracking: Proceedings of conference: September 11-15. The Ohio State University, Department of Mettalurgical Engineering. National Association of Corrosion Engineers; 1969. 1967.
[109] Bugaev VN, Gavriljuk VG, Petrov YuN, Tarasenko AV. Mechanism of hydrogen-induced phase transformations in metals and alloys. Int J Hydrogen Energy 1997;22(2–3):213–8. https://doi.org/10.1016/s0360-3199(96)00154-1.
[110] Głowacka A, Woźniak MJ, Nolze G, Świątnicki WA. Hydrogen induced phase transformations in austenitic-ferritic steel. Solid State Phenom 2006;112:133–40. https://doi.org/10.4028/www.scientific.net/ssp.112.133.
[111] Moriconi C, Hénaff G, Halm D. Cohesive zone modeling of fatigue crack propagation assisted by gaseous hydrogen in metals. Int J Fatig 2014;68:56–66. https://doi.org/10.1016/j.ijfatigue.2014.06.007.
[112] Jemblie L, Olden V, Akselsen OM. A review of cohesive zone modelling as an approach for numerically assessing hydrogen embrittlement of steel structures. Phil Trans Math Phys Eng Sci 2017;375(2098):20160411. https://doi.org/10.1098/rsta.2016.0411. 2098.
[113] Katzarov IH, Paxton AT. Hydrogen Embrittlement II. analysis of hydrogen-enhanced decohesion across (111) planes in α-Fe. Phys Rev Mater 2017;1(3). https://doi.org/10.1103/physrevmaterials.1.033603.
[114] Tehranchi A, Zhou X, Curtin WA. A decohesion pathway for hydrogen embrittlement in nickel: mechanism and Quantitative Prediction. Acta Mater 2020;185:98–109. https://doi.org/10.1016/j.actamat.2019.11.062.
[115] Birnbaum HK, Sofronis P. Hydrogen-enhanced localized plasticity—a mechanism for hydrogen-related fracture. Mater Sci Eng, A 1994;176(1–2):191–202. https://doi.org/10.1016/0921-5093(94)90975-x.
[116] Benbelaid S, Belouchrani MA, Assoul Y, Bezzazi B. Modeling damage of the hydrogen enhanced localized plasticity in stress corrosion cracking. Int J Damage Mech 2010;20(6):831–44. https://doi.org/10.1177/1056789510369327.
[117] Katzarov IH, Pashov DL, Paxton AT. Hydrogen Embrittlement I. Analysis of hydrogen-enhanced localized plasticity: effect of hydrogen on the velocity of screw dislocations in α-fe. Phys Rev Mater 2017;1(3). https://doi.org/10.1103/physrevmaterials.1.033602.
[118] Martin ML, Dadfarnia M, Nagao A, Wang S, Sofronis P. Enumeration of the hydrogen-enhanced localized plasticity mechanism for hydrogen embrittlement in structural materials. Acta Mater 2019;165:734–50. https://doi.org/10.1016/j.actamat.2018.12.014.
[119] Huang S, Zhang Y, Yang C, Hu H. Fracture strain model for hydrogen embrittlement based on hydrogen enhanced localized plasticity mechanism. Int J Hydrogen Energy 2020;45(46):25541–54. https://doi.org/10.1016/j.ijhydene.2020.06.271.
[120] Hatano M, Fujinami M, Arai K, Fujii H, Nagumo M. Hydrogen embrittlement of austenitic stainless steels revealed by deformation microstructures and strain-induced creation of vacancies. Acta Mater 2014;67:342–53. https://doi.org/10.1016/j.actamat.2013.12.039.
[121] Hattori M, Suzuki H, Seko Y, Takai K. The role of hydrogen-enhanced strain-induced lattice defects on hydrogen embrittlement susceptibility of X80 pipeline steel. JOM 2017;69(8):1375–80. https://doi.org/10.1007/s11837-017-2371-1.
[122] Nagumo M, Takai K. The predominant role of strain-induced vacancies in hydrogen embrittlement of steels: overview. Acta Mater 2019;165:722–33. https://doi.org/10.1016/j.actamat.2018.12.013.
[123] Murakami Y, Kanezaki T, Mine Y, Matsuoka S. Hydrogen embrittlement mechanism in fatigue of austenitic stainless steels. Metall Mater Trans 2008;39(6). https://doi.org/10.1007/s11661-008-9506-5.
[124] Martin ML, Sofronis P, Robertson IM, Awane T, Murakami Y. A microstructural based understanding of hydrogen-enhanced fatigue of stainless steels. Int J Fatig 2013;57:28–36. https://doi.org/10.1016/j.ijfatigue.2012.08.009.
[125] Brück S, Schippl V, Schwarz M, Christ H-J, Fritzen C-P, Weihe S. Hydrogen embrittlement mechanism in fatigue behavior of austenitic and martensitic stainless steels. Metals 2018;8(5):339. https://doi.org/10.3390/met8050339.
[126] Tabata T, Birnbaum H. Direct observations of the effect of hydrogen on the behavior of dislocations in iron. Scripta Metall 1983;17(7):947–50. https://doi.org/10.1016/0036-9748(83)90268-5.
[127] Robertson I, Birnbaum H. An HVEM study of hydrogen effects on the deformation and fracture of nickel. Acta Metall 1986;34(3):353–66. https://doi.org/10.1016/0001-6160(86)90071-4.
[128] Djukic MB, Bakic GM, Sijacki Zeravcic V, Rajicic B, Sedmak A, Mitrovic R, Miskovic Z. Towards a unified and practical industrial model for prediction of hydrogen embrittlement and damage in steels. Procedia Struct Integr 2016;3:604–11. https://doi.org/10.1016/j.prostr.2016.06.078.
[129] Wan L, Geng W, Ishii A, Du J, Mei Q, Ishikawa N, et al. Hydrogen embrittlement controlled by reaction of

Please cite this article as: Lee HW et al., Modeling fatigue life and hydrogen embrittlement of bcc steel with unified mechanics theory, International Journal of Hydrogen Energy, https://doi.org/10.1016/j.ijhydene.2023.02.110

dislocation with grain boundary in alpha-iron. Int J Plast 2019;112:206–19. https://doi.org/10.1016/j.ijplas.2018.08.013.
[130] Colla V, Valentini R. Assessment of critical hydrogen concentration in as-cast and hot-rolled billets in Medium Carbon Steels. Steel Res Int 2020;91(9):2000126. https://doi.org/10.1002/srin.202000126.
[131] Fangnon E, Yagodzinskyy Y, Malictki E, Mehtonen S, Virolainen E, Vilaça P. Determination of critical hydrogen concentration and its effect on mechanical performance of 2200 MPA and 600 HBW martensitic ultra-high-strength steel. Metals 2021;11(6):984. https://doi.org/10.3390/met11060984.
[132] Novak PM. A dislocation-based constitutive model for hydrogen-deformation interactions and a study of hydrogen-induced intergranular fracture (Order No. 3406790). 2009. Available from: ProQuest Dissertations & Theses Global. (288251968). Retrieved from, https://www.proquest.com/dissertations-theses/dislocation-based-constitutive-model-hydrogen/docview/288251968/se-2?accountid=14169.
[133] Novak P, Yuan R, Somerday B, Sofronis P, Ritchie R. A statistical, physical-based, micro-mechanical model of hydrogen-induced intergranular fracture in steel. J Mech Phys Solid 2010;58(2):206–26. https://doi.org/10.1016/j.jmps.2009.10.005.
[134] Hirth JP, Rice JR. On the thermodynamics of adsorption at interfaces as it influences decohesion. Metall Trans A 1980;11(9):1501–11. https://doi.org/10.1007/bf02654514.
[135] Nagao A, Dadfarnia M, Somerday BP, Sofronis P, Ritchie RO. Hydrogen-enhanced-plasticity mediated decohesion for hydrogen-induced intergranular and "quasi-cleavage" fracture of lath martensitic steels. J Mech Phys Solid 2018;112:403–30. https://doi.org/10.1016/j.jmps.2017.12.016.
[136] Dadfarnia Mohsen, Nagao Akihide, Somerday Brian P, Schembri Phillip E, James W, Foulk III, Nibur Kevin A, Balch Dorian K, Ritchie Robert O, Sofronis &Petros. Modeling hydrogen-induced fracture and crack propagation in high strength steels. In: Somerday BP, &Sofronis P, editors. International hydrogen conference (IHC 2016): materials performance in hydrogen environments. ASME Press; 2017. https://doi.org/10.1115/1.861387_ch65.
[137] Li X, Ma X, Zhang J, Akiyama E, Wang Y, Song X. Review of hydrogen embrittlement in metals: hydrogen diffusion, hydrogen characterization, hydrogen embrittlement mechanism and prevention. Acta Metall Sin 2020;33(6):759–73. https://doi.org/10.1007/s40195-020-01039-7.
[138] Smith E. The nucleation and growth of cleavage microcracks in mild steel, Physical Basis of Yield and Fracture, conf. Proc Inst Phys Phys Soc London 1966:36–46.
[139] McMahon C, Vitek V. The effects of segregated impurities on intergranular fracture energy. Acta Metall 1979;27(4):507–13. https://doi.org/10.1016/0001-6160(79)90002-6.
[140] Jokl M, Vitek V, McMahon C. A microscopic theory of brittle fracture in deformable solids: a relation between ideal work to fracture and plastic work. Acta Metall 1980;28(11):1479–88. https://doi.org/10.1016/0001-6160(80)90048-6.
[141] Birnbaum HK. Hydrogen effects on deformation and fracture: science and sociology. MRS Bull 2003;28(7):479–85. https://doi.org/10.1557/mrs2003.143.
[142] Benbelaid S, Belouchrani M, Assoul Y, Bezzazi B. Modeling damage of the hydrogen enhanced localized plasticity in stress corrosion cracking. Int J Damage Mech 2010;20(6):831–44. https://doi.org/10.1177/1056789510369327.
[143] Fernández-Sousa R, Betegón C, Martínez-Pañeda E. Analysis of the influence of microstructural traps on hydrogen assisted fatigue. Acta Mater 2020;199:253–63. https://doi.org/10.1016/j.actamat.2020.08.030.
[144] Isfandbod M, Martínez-Pañeda E. A mechanism-based multi-trap phase field model for hydrogen assisted fracture. Int J Plast 2021;144:103044. https://doi.org/10.1016/j.ijplas.2021.103044.
[145] Tateyama Y, Ohno T. Atomic-scale effects of hydrogen in iron toward hydrogen embrittlement: AB-Initio Study. ISIJ Int 2003;43(4):573–8. https://doi.org/10.2355/isijinternational.43.573.
[146] Pundt A, Kirchheim R. Hydrogen in metals: microstructural aspects. Annu Rev Mater Res 2006;36(1):555–608. https://doi.org/10.1146/annurev.matsci.36.090804.094451.
[147] Lin M, Yu H, Ding Y, Wang G, Olden V, Alvaro A, He J, Zhang Z. A predictive model unifying hydrogen enhanced plasticity and decohesion. Scripta Mater 2022;215:114707. https://doi.org/10.1016/j.scriptamat.2022.114707.
[148] McLellan RB. Solid solutions of hydrogen in gold, silver and copper. J Phys Chem Solid 1973;34(6):1137–41. https://doi.org/10.1016/s0022-3697(73)80022-8.
[149] Bukonte L, Ahlgren T, Heinola K. Thermodynamics of impurity-enhanced vacancy formation in metals. J Appl Phys 2017;121(4):045102. https://doi.org/10.1063/1.4974530.
[150] Mirzaev DA, Mirzoev AA, Okishev K Yu, Verkhovykh AV. Hydrogen–vacancy interaction in bcc iron: ab initio calculations and thermodynamics. Mol Phys 2013;112(13):1745–54. https://doi.org/10.1080/00268976.2013.861087.
[151] Sofronis P, McMeeking R. Numerical analysis of hydrogen transport near a blunting crack tip. J Mech Phys Solid 1989;37(3):317–50. https://doi.org/10.1016/0022-5096(89)90002-1.
[152] Krom A, Koers R, Bakker A. Hydrogen transport near a blunting crack tip. J Mech Phys Solid 1999;47(4):971–92. https://doi.org/10.1016/s0022-5096(98)00064-7.
[153] Zhu XD, Lee A, Wong A, Linke U. Surface diffusion of hydrogen on Ni(100): an experimental observation of quantum tunneling diffusion. Phys Rev Lett 1992;68(12):1862–5. https://doi.org/10.1103/physrevlett.68.1862.
[154] Sundell PG, Wahnström G. Self-trapping and diffusion of hydrogen in Nb and Ta from first principles. Phys Rev B 2004;70(22). https://doi.org/10.1103/physrevb.70.224301.
[155] Jiang DE, Carter EA. Diffusion of interstitial hydrogen into and through bcc Fe from first principles. Phys Rev B 2004;70(6). https://doi.org/10.1103/physrevb.70.064102.
[156] Kuwahata K, Hama T, Kouchi A, Watanabe N. Signatures of quantum-tunneling diffusion of hydrogen atoms on water ice at 10 K. Phys Rev Lett 2015;115(13). https://doi.org/10.1103/physrevlett.115.133201.
[157] Callister WD, Rethwisch DG. Materials science and engineering and introduction. John Wiley & Sons, Inc; 2007.
[158] Bai P, Zhou J, Luo B, Zheng S, Wang P, Tian Y. Hydrogen embrittlement of X80 pipeline steel in H2S environment: effect of hydrogen charging time, hydrogen-trapped state and hydrogen charging–releasing–recharging cycles. Int J Miner Metall Mater 2020;27(1):63–73. https://doi.org/10.1007/s12613-019-1870-1.
[159] Jemblie L, Olden V, Akselsen OM. A coupled diffusion and cohesive zone modelling approach for numerically assessing hydrogen embrittlement of steel structures. Int J Hydrogen Energy 2017;42(16):11980–95. https://doi.org/10.1016/j.ijhydene.2017.02.211.
[160] Nelson HG, Stein JE, Ames Research Center. *Gas-phase hydrogen permeation through alpha iron, 4130 steel, and 304 stainless steel from less than 100°C to near 600°C*. Washington, D.C: National Aeronautics and Space Administration; 1973.
[161] Yun H, Modarres M. Measures of entropy to characterize fatigue damage in metallic materials. Entropy 2019;21(8):804. https://doi.org/10.3390/e21080804.

Please cite this article as: Lee HW et al., Modeling fatigue life and hydrogen embrittlement of bcc steel with unified mechanics theory, International Journal of Hydrogen Energy, https://doi.org/10.1016/j.ijhydene.2023.02.110